Free excitons in wurtzite GaN

A. V. Rodina*

I. Physics Institute, Justus Liebig University of Giessen, 35392 Giessen, Germany

M. Dietrich, A. Göldner, L. Eckey, and A. Hoffmann

Solid State Physics Institute, Technical University of Berlin, D-10623, Berlin, Germany

Al. L. Efros and M. Rosen

Naval Research Laboratory, Washington DC 20375

B. K. Meyer

I. Physics Institute, Justus Liebig University of Giessen, 35392 Giessen, Germany

We present a comprehensive study of the free-exciton and exciton-polariton photoluminescence in wurtzite GaN. Using polarization-dependent measurements we were able to resolve the fine-structure energy splittings in the $n=1$ state of the A exciton and to determine the energy separation between the $1S$ and $2P_{\pm 1}$ states as 19.7 ± 0.2 meV. For the $n=1$ state, the evolution of the emission from two transverse polariton branches Γ_{5T1} and Γ_{5T2}, the longitudinal exciton Γ_{5L}, and the dipole-forbidden exciton Γ_6 in magnetic fields up to 15 T have been studied in Faraday configuration. We have estimated the value of the parallel effective g factor of the hole mixed into the $1S$ state of the A exciton as $g_{A,1S}^{\parallel} = 2.25 \pm 0.2$. To describe these data a theory is developed for the exciton energy structure in hexagonal semiconductors with wurtzite symmetry in zero and in weak external magnetic fields which takes into account the effect of the hexagonal lattice anisotropy and the coupling of all excitonic states belonging to different valence subbands. The effect of the exciton interaction with polar optical phonons is considered. The theory is very successful in describing the free-exciton emission and magnetoluminescence in wurtzite GaN. The effective mass parameters and the magnetic Luttinger constant as well as the effective Rydberg numbers and binding energies of the A, B, and C excitons are determined from a comparison of the theory with experimental data.

I. INTRODUCTION

In the past decade, much attention has been paid to the physics and optical properties of the group-III nitrides, such as GaN, InN, and AlN and their ternary alloys. This is because it is the basic material for blue lasers and light emitting diodes (LED's).[1] The determination of the energy structure and effective mass parameters of wurtzite GaN has been the focus of many experimental and theoretical studies.[2–14] However, the values of the exciton effective Rydberg numbers, hole effective masses, and g values as well as the excitonic fine-structure splittings reported so far exhibit considerable scatter. This is caused both by experimental difficulties and by the lack of an appropriate theoretical description of the exciton energy structure.

The main factor that makes the exciton structure in wurtzite GaN different and which requires a more complicated theoretical analysis from those in the well-studied wide gap II-VI semiconductors is that the energy separation between the valence subbands A, B, and C is smaller than or of the same order as the exciton binding energies (see Fig. 1). The coupling of the exciton states belonging to different subbands can strongly influence exciton transition energies[15,16] and reflection properties.[17] Exciton transition energies and valence subband splittings are known to be influenced by biaxial strain always present in GaN films.[10,18–21] Therefore, the effect of strain and the effect of intersubband coupling must be taken into account for a proper understanding of the optical spectra and the extraction of the basic parameters in wurtzite GaN.

Several reasons have prevented the observation of the exciton fine structure in GaN until now. First, hexagonal epitaxial GaN layers have their c axis parallel to the growth direction, which is perpendicular to the layer surface. In normal optical–transmission experiments this allows the detection only of light with a polarization perpendicular to the c axis and does not allow the detection of weak "forbidden" absorption lines which was possible in CdS.[22,23] Second, reflection spectra in GaN are broadened significantly due to the high defect concentration in the layers and do not allow one to obtain much information on the energy fine structure. Third, many optical investigations of GaN have been limited in accuracy and detail due to large linewidths, more than 2 meV, which are caused by the extremely large mismatch between the GaN epilayer and the substrate, which leads to an inhomogeneous biaxial strain and a large number of structural defects.

Most data on exciton effective Rydberg numbers published to date have been obtained from the experimentally observed separation between the $n=1$ ground and the $n=2$ first excited exciton states,[9,11–14,24,25] where the simplest hydrogenlike or anisotropic[22,26] models of the three uncoupled excitons have been used. However, the binding energies of the $n=1$ exciton states in other semiconductors were shown
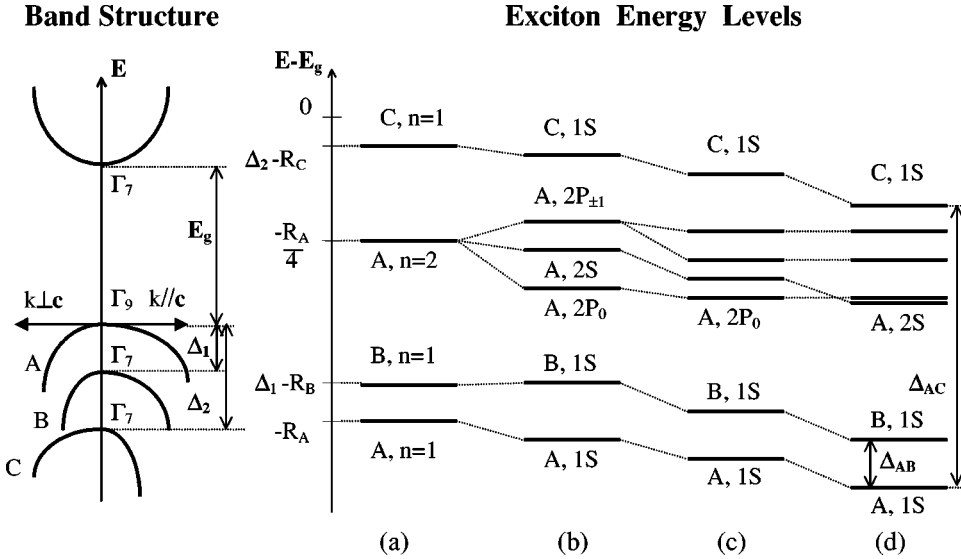
FIG. 1. A schematic of the energy band structure and exciton energy levels in wurtzite GaN in (a) an uncoupled hydrogenlike isotropic model, (b) including the effect of anisotropy, (c) including the effects both of anisotropy and intersubband coupling, and (d) including anisotropy, intersubband coupling, and polaron corrections.

to differ from the Rydberg energy by several meV.[15] In addition, the interpretations given by different groups of the observed emission lines in the region of the $n = 2$ state of the A and B excitons vary considerably, resulting in a large scatter of the determined exciton effective Rydberg numbers. Thus, a careful identification of the emission lines observed as well as a proper theoretical description of the exciton energy levels in wurtzite GaN is needed for the correct determination of the exciton effective Rydberg numbers.

A perturbational approach for calculating exciton energy levels in zero and weak external magnetic fields for the case of a degenerate valence band was developed some time ago, and successfully applied to $1S$ and $2S$ states in diamond and zinc-blende semiconductors.[27–30] This approach was extended to treat exciton ground-state levels in zero magnetic field in wurtzite-type semiconductors[31,15] and revealed the importance of the intersubband coupling corrections to the ground-state energy in CdS.[15]

Moreover, the effect of polar interactions with optical phonons must be considered because of the large ionicity of GaN. A large lattice contribution to the screening dielectric constant[32,33] suggests that the screening of the effective interaction between electrons and holes in an exciton must be described by a spatially dependent dielectric constant.[34–39] For a number of polar semiconductors, this results in large polaron corrections to both the exciton binding energies and the values of the exciton diamagnetic shifts in external magnetic fields. A full description of the exciton-optical phonon system in anisotropic semiconductors having a small separation between valence subbands is very complicated, and an appropriate model for the polaron corrections in wurtzite GaN is yet to be developed.

In the present paper we study the exciton and exciton–polariton fine structure in wurtzite GaN and its evolution in an external magnetic field of strength up to $H = 15$ T. We do this for both $\mathbf{H} \| c$ and $\mathbf{H} \perp c$ in Faraday configuration. Our high-quality samples allowed us to observe the zero–phonon exciton emission line in the low-temperature photoluminescence (PL) spectra from the surface and the side faces that are thick enough for the separate detection of luminescence

polarized parallel or perpendicular to the c axis. To interpret the data, we develop a theory of the ground and excited exciton energy levels for hexagonal semiconductors having wurtzite symmetry in zero and weak external magnetic fields. Using model wurtzite GaN parameters, we investigate the importance of the anisotropy and intersubband coupling corrections, as well as the effect of biaxial strain on the exciton binding energies and hole effective g factors. To estimate the polaron corrections to the exciton energy levels in GaN, we compare three effective polaron models that are similar to those known for semiconductors with a simple band structure.[34–38] This analysis allows us to determine a range of appropriate band and polaron effective mass parameters and magnetic constants in wurtzite GaN.

The paper is organized in the following way. Section II is devoted to the theory of free excitons in hexagonal semiconductors. It includes a description of the model (Sec. II A) and of the perturbation Hamiltonian (Sec. II B), a calculation of the exciton energy levels in zero (Sec. II C) and weak (Sec. II D) magnetic fields, and, finally, a description of the A exciton-polariton fine structure in zero and weak magnetic fields (Sec. II E). Section III describes the samples and the experimental techniques we used. In Sec. IV we give an overview of the complete unpolarized exciton PL spectrum in GaN (Sec. IV A) and present the measurements of the A exciton polarized emission, revealing the complete fine structure of the $n = 1$ state in zero and weak magnetic fields (Sec. IV B) and the position of the $2P_{\pm 1}$ sublevel (Sec. IV C). In Sec. V we compare the experimental data with the theory, discuss the effect of the interaction with optical phonons (Sec. V A), and evaluate the effective-mass and magnetic parameters of GaN (Sec. V B). In Sec. VI we compare our results with those already published.

II. THEORY OF FREE EXCITONS IN HEXAGONAL SEMICONDUCTORS

A. Model of direct excitons

The Hamiltonian of the relative electron–hole motion in a magnetic field in a hexagonal semiconductor is

$$\hat{H}_{exc}(\mathbf{k})=\hat{H}_e\left(\mathbf{k}+\frac{e}{\hbar c}\mathbf{A}\right)-\hat{H}_h\left(-\mathbf{k}+\frac{e}{\hbar c}\mathbf{A}\right)$$

$$-\frac{e^2}{\sqrt{\varepsilon_0^{\parallel}\varepsilon_0^{\perp}(x^2+y^2)+\varepsilon_0^{\perp2}z^2}}, \tag{1}$$

where $\mathbf{k}=-i\nabla$ is the wave vector of the relative motion, $(x,y,z)=(\mathbf{r})$ are the relative electron-hole coordinates (the z direction is chosen along the hexagonal c axis), e is the magnitude of the free-electron charge, $\varepsilon_0^{\parallel}$ and $\varepsilon_0^{\perp}$ are the low-frequency dielectric constants, and $\mathbf{A}=(1/2)[\mathbf{H}\times\mathbf{r}]$ is the vector potential of the magnetic field. We write the kinetic energy parts of the electron, $\hat{H}_e$, and hole, $\hat{H}_h$, Hamiltonians in a quasicubic approximation,[40] neglecting relativistic terms linear in $\mathbf{k}$:

$$\hat{H}_e(\mathbf{k})=\frac{\hbar^2}{2m_e^{\parallel}}k_z^2+\frac{\hbar^2}{2m_e^{\perp}}(k_x^2+k_y^2)+\frac{1}{2}g_e^{\parallel}\mu_B(\hat{\sigma}_zH_z)$$

$$+\frac{1}{2}g_e^{\perp}\mu_B(\hat{\sigma}_xH_x+\hat{\sigma}_yH_y), \tag{2}$$

$$-\hat{H}_h(\mathbf{k})=\frac{\hbar^2}{2m_0}\left[(\gamma_1+4\gamma)k^2-6\gamma\left(\sum_{\alpha=x,y,z}k_\alpha^2\hat{I}_\alpha^2\right.\right.$$

$$\left.\left.+2\sum_{\alpha\neq\beta}\{k_\alpha k_\beta\}\{\hat{I}_\alpha\hat{I}_\beta\}\right)\right]-\frac{1}{3}\Delta_{so}^{\parallel}[(\hat{I}_z\hat{\sigma}_z)-1]$$

$$-\frac{1}{3}\Delta_{so}^{\perp}(\hat{I}_\perp\hat{\sigma}_\perp)-\Delta_{cr}[\hat{I}_z^2-1]-\mu_B(1+3\kappa)(\hat{I}\mathbf{H})$$

$$+\frac{1}{2}\mu_Bg_0(\hat{\sigma}\mathbf{H}), \tag{3}$$

where m_0 and $g_0=2$ are the free electron mass and g factor, respectively, $m_e^{\parallel}$ ($m_e^{\perp}$) and $g_e^{\parallel}$ ($g_e^{\perp}$) are the parallel (perpendicular) values of the electron effective masses and g factors respectively, $\mu_B=e\hbar/2m_0c$ is the Bohr magneton, $\hat{\sigma}_{x,y,z}$ are the Pauli matrices, $\hat{\mathbf{I}}$ is the orbital angular momentum operator of the hole ($I=1$), $\{ab\}=(ab+ba)/2$, γ_1 and $\gamma=\gamma_2=\gamma_3$ are the effective mass Luttinger parameters,[41] and κ is the magnetic Luttinger constant[41] of the quasicubic approximation. The crystal field energy Δ_{cr} and the spin-orbit coupling parameters $\Delta_{so}^{\parallel}$ and $\Delta_{so}^{\perp}$ are connected with the zero-field splittings of the valence subbands A, B, and C at $k=0$ by[40]

$$\Delta_{1,2}=\frac{1}{2}\left[\Delta_{so}^{\parallel}+\Delta_{cr}\mp\sqrt{\left(\Delta_{cr}-\frac{\Delta_{so}^{\parallel}}{3}\right)^2+\frac{8}{9}\Delta_{so}^{\perp2}}\right], \tag{4}$$

where the upper sign ($-$) is used for the A-B separation and the lower ($+$) for the A-C split. We note that Eq. (3) takes into account the hexagonal anisotropy of the spin-orbit interaction. This is essential for accurately describing the valence band splittings at the Γ point in wurtzite GaN and their dependence on an external biaxial strain.[18] The latter does not change the wurtzite symmetry[10,18] and can be taken into account within the model by writing[21] $\Delta_{cr}=\Delta_{cr}^0+\delta_{cr}$, $E_g=E_g^0+\delta_g$, where E_g is the band gap, δ_{cr} and δ_g are each proportional to the biaxial stress, and Δ_{cr}^0 and E_g^0 are the values of the respective parameters for zero stress.

We choose the 12 wurtzite-symmetry basis functions of the A, B, and C exciton states as

$$u_A^+u_e^+,u_A^-u_e^+,u_B^+u_e^+,u_B^-u_e^+,u_C^+u_e^+,u_C^-u_e^+,u_A^+u_e^-,u_A^-u_e^-,u_B^+u_e^-,u_B^-u_e^-,u_C^+u_e^-,u_C^-u_e^-, \tag{5}$$

where $u_e^{\pm}$ are the Γ–point Bloch functions of the electron in the conduction band, and $u_v^{\pm}$ ($v=A$, B, and C) are those of the hole in the valence subbands. Below we show the symmetry, energy, and the explicit form of the Bloch wave functions of corresponding electron and hole states at $k=0$:

Symmetry	Energy		
Γ_7	E_g	$u_e^+=\|S\rangle\uparrow,$	$u_e^-=i\|S\rangle\downarrow,$
Γ_9	0	$u_A^+=\|1,1\rangle\uparrow,$	$u_A^-=i\|1,-1\rangle\downarrow,$
Γ_7	$-\Delta_1$	$u_B^+=ia\|1,1\rangle\downarrow-ib\|1,0\rangle\uparrow,$	$u_B^-=a\|1,-1\rangle\uparrow+b\|1,0\rangle\downarrow,$
Γ_7	$-\Delta_2$	$u_C^+=ib\|1,1\rangle\downarrow+ia\|1,0\rangle\uparrow,$	$u_C^-=b\|1,-1\rangle\uparrow-a\|1,0\rangle\downarrow.$

Here $|1,\pm1>=(|X\rangle\pm i|Y\rangle)/\sqrt{2}$, $|1,0\rangle=|Z\rangle$ (in wurtzite symmetry the function $|S\rangle$ may have some admixture of $|Z\rangle$ character), and the coefficients a and b are

$$a=\frac{1}{\sqrt{x^2+1}},\quad b=\frac{x}{\sqrt{x^2+1}},\quad x=\frac{-(3\Delta_{cr}-\Delta_{so}^{\parallel})+\sqrt{(3\Delta_{cr}-\Delta_{so}^{\parallel})^2+8\Delta_{so}^{\perp2}}}{2\sqrt{2}\Delta_{so}^{\perp}}. \tag{6}$$

B. Perturbation Hamiltonians

To adapt the perturbation method developed in Refs. 27 and 28 for cubic semiconductors, we first rescale the coordinates $x\rightarrow x$, $y\rightarrow y$, and $z\rightarrow z\sqrt{\eta}$, where $\eta=\varepsilon_0^{\perp}/\varepsilon_0^{\parallel}$. The Coulomb interaction term then becomes spherically symmetric and equal to $-e^2/\varepsilon_0 r$, with $\varepsilon_0=\sqrt{\varepsilon_0^{\perp}\varepsilon_0^{\parallel}}$. The exciton Hamiltonian (1) can then be written as $\hat{H}_{exc}=\hat{H}_s+\hat{H}_d+\hat{H}_l+\hat{H}_q$, where $\hat{H}_s$ and $\hat{H}_d$

are the s–like and d–like parts of the Hamiltonian describing the A, B, and C excitons in a zero magnetic field, and the operators $\hat{H}_l$ and $\hat{H}_q$ describe the effect of a magnetic field and contain terms linear and quadratic in the magnetic field, respectively. The operators $\hat{H}_s$ and $\hat{H}_d$ do not mix the exciton basis functions containing u_e^+ and those containing u_e^- and can be written as $\hat{H}_s = \hat{H}_0 + \hat{H}_{coup}^s$ and $\hat{H}_d = \hat{H}_{an} + \hat{H}_{coup}^d$. The Hamiltonian $\hat{H}_0$ describes uncoupled A, B, and C exciton states in isotropic approximation, and $\hat{H}_{an}$ describes the effect of anisotropy,

$$\hat{H}_0 = \begin{vmatrix} \hat{H}_A^0 \hat{T}_2 & 0 & 0 \\ 0 & (\Delta_1 + \hat{H}_B^0)\hat{T}_2 & 0 \\ 0 & 0 & (\Delta_2 + \hat{H}_C^0)\hat{T}_2 \end{vmatrix}, \quad \hat{H}_{an} = \begin{vmatrix} \hat{H}_A^{an}\hat{T}_2 & 0 & 0 \\ 0 & \hat{H}_B^{an}\hat{T}_2 & 0 \\ 0 & 0 & \hat{H}_C^{an}\hat{T}_2 \end{vmatrix}, \tag{7}$$

where $\hat{T}_2$ is the 2×2 unit matrix and

$$\hat{H}_v^0 = \frac{\hbar^2 k^2}{2\mu_v} - \frac{e^2}{\varepsilon_0 r}, \quad \hat{H}_v^{an} = \frac{\hbar^2(k^2 - 3k_z^2)}{2\mu_v^{an}}, \quad v = A,B,C, \tag{8}$$

$$\frac{1}{\mu_v} = \frac{1}{3}\left[\frac{2}{\mu_v^\perp} + \frac{\eta}{\mu_v^\parallel}\right], \quad \frac{1}{\mu_v^{an}} = \frac{1}{3}\left[\frac{1}{\mu_v^\perp} - \frac{\eta}{\mu_v^\parallel}\right], \quad \frac{1}{\mu_v^\perp} = \frac{1}{m_e^\perp} + \frac{1}{m_v^\perp}, \quad \frac{1}{\mu_v^\parallel} = \frac{1}{m_e^\parallel} + \frac{1}{m_v^\parallel}. \tag{9}$$

The hole effective masses in the valence subbands $m_v^{\parallel,\perp}$ ($v = A,B,C$) are given by[40,10]

$$\frac{m_0}{m_A^\parallel} = (\gamma_1 - 2\gamma), \quad \frac{m_0}{m_A^\perp} = (\gamma_1 + \gamma), \tag{10}$$

$$\frac{m_0}{m_B^\parallel} = \left[\gamma_1 + \gamma\left(1 - \frac{3\Delta_{cr} - \Delta_{so}^\parallel}{\Delta_2 - \Delta_1}\right)\right], \quad \frac{m_0}{m_B^\perp} = \left[\gamma_1 - \frac{1}{2}\gamma\left(1 - \frac{3\Delta_{cr} - \Delta_{so}^\parallel}{\Delta_2 - \Delta_1}\right)\right], \tag{11}$$

$$\frac{m_0}{m_C^\parallel} = \left[\gamma_1 + \gamma\left(1 + \frac{3\Delta_{cr} - \Delta_{so}^\parallel}{\Delta_2 - \Delta_1}\right)\right], \quad \frac{m_0}{m_C^\perp} = \left[\gamma_1 - \frac{1}{2}\gamma\left(1 + \frac{3\Delta_{cr} - \Delta_{so}^\parallel}{\Delta_2 - \Delta_1}\right)\right]. \tag{12}$$

The values μ_v are the reduced masses averaged over the three directions in **k** space and the ratios $p_v = \mu_v / \mu_v^{an}$ are a measure of the anisotropy of the A, B, and C exciton reduced masses, respectively. The Hamiltonians $\hat{H}_{coup}^s$ and $\hat{H}_{coup}^d$ describe the coupling between exciton states belonging to different subbands:

$$\hat{H}_{coup}^s = \gamma\frac{\hbar^2 k^2}{m_0}(1-\eta)ab \times \begin{vmatrix} 0 & 0 & 0 \\ 0 & 0 & \hat{T}_2 \\ 0 & \hat{T}_2 & 0 \end{vmatrix} \tag{13}$$

and

$$\hat{H}_{coup}^d = \gamma \times \begin{vmatrix} 0 & 0 & b\sqrt{\eta}Q_1 & aQ_2 & -a\sqrt{\eta}Q_1 & bQ_2 \\ 0 & 0 & aQ_2^+ & -b\sqrt{\eta}Q_1^+ & b\sqrt{\eta}Q_2^+ & a\sqrt{\eta}Q_1^+ \\ b\sqrt{\eta}Q_1^+ & aQ_2 & 0 & 0 & ab(1+2\eta)Q & -\sqrt{\eta}Q_1 \\ aQ_2^+ & -b\sqrt{\eta}Q_1 & 0 & 0 & \sqrt{\eta}Q_1^+ & ab(1+2\eta)Q \\ -a\sqrt{\eta}Q_1^+ & bQ_2 & ab(1+2\eta)Q & \sqrt{\eta}Q_1 & 0 & 0 \\ bQ_2^+ & a\sqrt{\eta}Q_1 & -\sqrt{\eta}Q_1^+ & ab(1+2\eta)Q & 0 & 0 \end{vmatrix}, \tag{14}$$

where

$$Q = \frac{\hbar^2}{2m_0}(k^2 - 3k_z^2), \quad Q_1 = -i\frac{3\sqrt{2}\hbar^2}{2m_0}k_-k_z, \quad Q_2 = \frac{3\hbar^2}{2m_0}k_-^2, \quad k_\pm = (k_x \pm ik_y). \tag{15}$$

The coupling parameter is $p_h = \gamma \mu_0 / m_0$, where μ_0 is the exciton reduced mass averaged over the three directions in **k** space and over the A, B, and C excitons:

$$\frac{1}{\mu_0} = \frac{1}{3}\left[\frac{1}{\mu_A} + \frac{1}{\mu_B} + \frac{1}{\mu_C}\right]. \tag{16}$$

For the small values of p_v and p_h, the anisotropy $\hat{H}_{an}$ and coupling $\hat{H}_{coup} = \hat{H}^s_{coup} + \hat{H}^d_{coup}$ Hamiltonians can be treated perturbationally.

C. Exciton energy levels at zero field

The exact solutions of the isotropic unperturbed Hamiltonian H_0 are hydrogenlike A, B, and C exciton wave functions:

$$\Psi^{v\pm}_{[n,k],l,m} u^\pm_e = Y_{l,m}(\mathbf{r}/r) R_{[n,k],l}(r/a_v) u^\pm_v u^\pm_e, \quad v = A,B,C, \tag{17}$$

where the $Y_{l,m}$ are spherical harmonics and $R_{[n,k],l}$ are hydrogen radial wave functions for discrete ($n = 1,2,3 \dots$) and continuous spectra[42] with effective Bohr radii $a_v = \hbar^2 \varepsilon_0 / e^2 \mu_v$. The remaining part of the Hamiltonian can be considered as a perturbation. To second order in the perturbation one can find the energies of the A, B, and C exciton states in zero magnetic field:

$$E^0_{A,n,l,m} = E_g - E^{bind}_{A,n,l,m},$$

$$E^0_{B,n,l,m} = E_g + \Delta_1 - E^{bind}_{B,n,l,m}, \tag{18}$$

$$E^0_{C,n,l,m} = E_g + \Delta_2 - E^{bind}_{C,n,l,m},$$

where

$$E^{bind}_{v,n,l,m} = \frac{1}{n^2}(R_v + \Delta E^{an}_{v,n,l,m} + \Delta E^{coup}_{v,n,l,m}), \quad v = A,B,C, \tag{19}$$

and $R_v = \mu_v e^4 / 2\hbar^2 \varepsilon_0^2$ are the effective Rydberg numbers of the A, B, and C excitons, respectively. The terms $\Delta E^{an}_{v,n,l,m}$ and $\Delta E^{coup}_{v,n,l,m}$ contain the anisotropy and intersubband coupling corrections, respectively. For the S and P exciton states the anisotropy energy corrections $\Delta E^{an}_{v,n,l,m}$ can be written as

$$S(l=0) : \Delta E^{an}_{v,n}(S) = R_v \frac{16}{5n} p_v^2 S_n(0), \tag{20}$$

$$P_0(l=1, m=0):$$

$$\Delta E^{an}_{v,n}(P_0) = R_v\left[\frac{4}{5}p_v + 4p_v^2\left(P^1_n(0) + \frac{9}{4}P^3_n(0)\right)\right], \tag{21}$$

$$P_{\pm 1}(l=1, m=\pm 1):$$

$$\Delta E^{an}_{v,n}(P_{\pm 1}) = R_v\left[-\frac{2}{5}p_v + p_v^2(P^1_n(0) + 6P^3_n(0))\right], \tag{22}$$

where the functions $S_{n=1,2}$ (which were defined previously in Ref. 27), $P^1_{n=2}$, and $P^3_{n=2}$ are given in Appendix A.

In deriving the intersubband coupling energy corrections $\Delta E^{coup}_{v,n}$ we have used the same effective Bohr radius $a_0 = \hbar^2 \varepsilon_0 / e^2 \mu_0$ and effective Rydberg number $R_0 = \mu_0 e^4 / 2\hbar^2 \varepsilon_0^2$ averaged over the A, B, and C excitons for all three exciton series. For the $1S$ and $2S$ states of the A, B, and C excitons the coupling energy corrections are

$$\Delta E^{coup}_{A,n}(S) = R_0 \frac{48}{5n} p_h^2 [(2a^2 + \eta b^2) S_n(\Delta^0_1) + (\eta a^2 + 2b^2) S_n(\Delta^0_2)], \tag{23}$$

$$\Delta E^{coup}_{B,n}(S) = R_0 \frac{48}{5n} p_h^2 [(2a^2 + \eta b^2) S_n(-\Delta^0_1) + (\eta + a^2 b^2) S_n(\Delta^0_2 - \Delta^0_1)], \tag{24}$$

$$\Delta E^{coup}_{C,n}(S) = R_0 \frac{48}{5n} p_h^2 [(\eta a^2 + 2b^2) S_n(-\Delta^0_2) + (\eta + a^2 b^2) S_n(\Delta^0_1 - \Delta^0_2)], \tag{25}$$

where $\Delta^0_{1,2} = \Delta_{1,2}/R_0$, $n = 1,2$. In Eqs. (24) and (25) we neglect the corrections to the B and C exciton states coming from H^s_{coup} because they are proportional to $p_h^2(1-\eta)^2$ and are numerically small.

We will focus now on the $2P$ states of the A exciton. The intersubband coupling leads to a splitting of the $P_{\pm 1}$ states. We denote the resulting states $P^{1/2}_{\pm 1}$ and $P^{5/2}_{\pm 1}$. The former are described by the wave functions $\Psi^{A\mp}_{n,1,\pm 1}$ ($m=1, u^-_v u^\pm_e$ and $m=-1, u^+_v u^\pm_e$) and the latter by $\Psi^{A\pm}_{n,1,\pm 1}$ ($m=1, u^+_v u^\pm_e$ and $m=-1, u^-_v u^\pm_e$, respectively). The corresponding energy corrections to the $2P$ states of the A exciton are

$$\Delta E^{coup}_{A,n=2}(P_0) = R_0 \times 3p_h^2\{\eta b^2[3\tilde{P}^1_n(\Delta^0_1) + 8P^3_n(\Delta^0_1)] + a^2 10 P^3_n(\Delta^0_1) + \eta a^2[3\tilde{P}^1_n(\Delta^0_2) + 8P^3_n(\Delta^0_2)] + b^2 10 P^3_n(\Delta^0_2)\}, \tag{26}$$

$$\Delta E^{coup}_{A,n=2}(P^{1/2}_{\pm 1}) = R_0 \times 3p_h^2\{\eta b^2[\tilde{P}^1_n(\Delta^0_1) + P^3_n(\Delta^0_1)] + 2a^2[6\tilde{P}^1_n(\Delta^0_1) + P^3_n(\Delta^0_1)] + \eta a^2[\tilde{P}^1_n(\Delta^0_2) + P^3_n(\Delta^0_2)] + 2b^2[6\tilde{P}^1_n(\Delta^0_2) + P^3_n(\Delta^0_2)]\}, \tag{27}$$

$$\Delta E^{coup}_{A,n=2}(P^{5/2}_{\pm 1}) = R_0 \times 30 p_h^2[\eta b^2 P^3_n(\Delta^0_1) + 3a^2 P^3_n(\Delta^0_1) + \eta a^2 P^3_n(\Delta^0_2) + 3b^2 P^3_n(\Delta^0_2)], \tag{28}$$

where $\tilde{P}^1_{n=2}(x) = 1/(25x) + P^1_{n=2}(x)$ is defined for $x \neq 0$.

The structure of the A, B, and C exciton ground states ($n = 1$) and of the excited ($n = 2$) states of the A exciton, obtained in the hydrogenlike isotropic model with corrections arising from anisotropy and intersubband coupling, is shown in Fig. 1. In analyzing the significance of these effects and their dependence on biaxial stress in wurtzite GaN, we used the spin–orbit coupling constants $\Delta^\|_{so} = 18.5$ meV and

TABLE I. Energy corrections to the A, B, and C ground $n=1$ state exciton levels in zero magnetic field for three sets of model GaN parameters. The parameters used are $\Delta_{so}^{\parallel}=18.5$ meV, $\Delta_{so}^{\perp}=17.1$ meV, $\eta=0.92$, $m_e^{\parallel}=m_e^{\perp}=0.22m_0$ and $R_0=26.0$ meV for sets (i)–(iii) and (i) $p_h=0.05$, $\Delta_{cr}=8.0$ meV, (ii) $p_h=0.1$, $\Delta_{cr}=8.0$ meV, (iii) $p_h=0.1$, $\Delta_{cr}=18.0$ meV.

	R_A (meV)	R_B (meV)	R_C (meV)	p_A	p_B	p_C	ΔE_A^{an} (meV)	ΔE_B^{an} (meV)	ΔE_C^{an} (meV)	ΔE_A^{coup} (meV)	ΔE_B^{coup} (meV)	ΔE_C^{coup} (meV)
(i)	25.94	26.03	26.06	0.075	0.01	0.075	0.10	0.003	0.10	0.34	0.36	0.68
(ii)	25.86	26.05	26.1	0.12	0.004	0.16	0.28	0.	0.29	1.42	1.52	2.86
(iii)	25.86	25.95	26.2	0.12	0.07	0.12	0.28	0.08	0.30	1.37	1.71	2.46

$\Delta_{so}^{\perp}=17.1$ meV and took as the value of the average exciton Rydberg number $R_0=26.0$ meV. As the exciton binding energies, $\propto R_0$, are smaller than those of optical phonons in GaN, $E_{lo}=91.5$ meV,[32,33] we replace the electron effective masses by those for polarons, $m_e^{\parallel *}=m_e^{\perp *}=m_e^*=0.22m_0$,[6,43] and use static dielectric constants taken from Refs. 32 and 33 to obtain $\eta \approx 0.92$. We calculated the values of the anisotropy parameters, the exciton Rydberg numbers, and the resulting energy corrections for three different pairs of values of the coupling parameters and crystal field energy: (i) $p_h=0.05$, $\Delta_{cr}=8.0$ meV, (ii) $p_h=0.1$, $\Delta_{cr}=8.0$ meV, and (iii) $p_h=0.1$, $\Delta_{cr}=18.0$ meV. The results are given in Tables I and II. One can see that the coupling correction in GaN is more significant than the effect of anisotropy. The same result has been obtained for the ground states of the A and B excitons in CdS.[15] The stress dependence of the coupling corrections is more pronounced for the ground state of the B and C excitons and for the $2P$ states of the A exciton.

The perturbation approach is valid if the energy corrections satisfy $(\Delta E_{v,n=1}^{an}+\Delta E_{v,n=1}^{coup})<\frac{3}{4}R_v$ and $(\Delta E_{v,n=2}^{an}+\Delta E_{v,n=2}^{coup})<\frac{5}{9}R_v$, for $v=A,B,C$. These conditions hold for the GaN parameters we used (see Tables I and II). We can compare our anisotropy energy corrections with those obtained numerically in Refs. 44–47. For a value of the anisotropy parameter $p_v=0.25$, our results agree with those of Ref. 47 to within 1% for the ground state and 2% for the excited exciton states. The intersubband coupling parameters p_h are defined in the same way and are of the same order of magnitude as those in semiconductors with a degenerate valence band.[27,29,30] Therefore, the accuracy of a perturbation treatment of the intersubband coupling in wurtzite semiconductors[48] is expected to be the same as that found for zinc–blende semiconductors.[27]

D. Exciton energy levels in a weak magnetic field

We now consider the effect of a weak external magnetic field H on the exciton energy structure. It can can be treated

pertubatively together with $\hat{H}_{an}$ and $\hat{H}_{coup}$ if the condition $\gamma_H=\mu_B H/\mu_0 R_0 \lesssim 0.4$ is satisfied.[28] For GaN, a value of $\gamma_H \approx 0.2$ corresponds to a magnetic field $H=15$ T. We consider a magnetic field with components perpendicular and parallel to the hexagonal axis, $\mathbf{H}=(H_x,0,H_z)$, and restrict ourselves to linear Zeeman effects only. We can write $\hat{H}_l$, in the basis of Eq. (5), as

$$\hat{H}_l=\frac{1}{2}\mu_B(\hat{G}_e^{\parallel}H_z+\hat{G}_e^{\perp}H_x)+\frac{1}{2}\mu_B(\hat{G}_h^{\parallel}H_z+\hat{G}_h^{\perp}H_x)$$
$$+\mu_B(\hat{G}_{or}^{\parallel}H_z+\hat{G}_{or}^{\perp}H_x)+\mu_B\hat{G}_{an}H_x+\mu_B(\hat{G}_{coup}^{\parallel}H_z$$
$$+\hat{G}_{coup}^{\perp}H_x), \qquad (29)$$

where the electron operators $\hat{G}_e^{\parallel,\perp}$ are diagonal in the hole basis functions $u_v^{\pm}$ and, in the basis of the electron Bloch functions u_e^+ and u_e^-, are given by $\hat{G}_e^{\parallel}=g_e^{\parallel}\hat{\sigma}_z$ and $\hat{G}_e^{\perp}=ig_e^{\perp}\hat{\sigma}_x$. All other operators in Eq. (29) are diagonal in the electron basis functions. The hole operators $\hat{G}_h^{\parallel,\perp}$ in the basis of the six exciton functions $u_v^{\pm}u_e^+$ (or $u_v^{\pm}u_e^-$) are

$$\hat{G}_h^{\parallel}=\begin{vmatrix} g_A^{\parallel}\hat{\sigma}_z & 0 & 0 \\ 0 & g_B^{\parallel}\hat{\sigma}_z & g_{BC}^{\parallel}\hat{\sigma}_z \\ 0 & g_{BC}^{\parallel}\hat{\sigma}_z & g_C^{\parallel}\hat{\sigma}_z \end{vmatrix},$$

$$\hat{G}_h^{\perp}=i\begin{vmatrix} g_A^{\perp}\hat{\sigma}_x & g_{AB}^{\perp}\hat{\sigma}_z & g_{AC}^{\perp}\hat{\sigma}_z \\ g_{AB}^{\perp}\hat{\sigma}_z & g_B^{\perp}\hat{\sigma}_x & g_{BC}^{\perp}\hat{\sigma}_x \\ \hat{g}_{AC}^{\perp}\hat{\sigma}_z & g_{BC}^{\perp}\hat{\sigma}_x & g_C^{\perp}\hat{\sigma}_x \end{vmatrix}, \qquad (30)$$

where the parallel and perpendicular effective hole g factors for the uncoupled A, B, and C subbands are

TABLE II. Energy corrections to the A-exciton energy levels in zero magnetic field. The GaN model parameters used are the same as in Table I.

	R_A (meV)	p_A	ΔE_A^{an} (meV)				ΔE_A^{coup} (meV)				
			$(1S)$	$(2S)$	$(2P_0)$	$(2P_\pm)$	$(1S)$	$(2S)$	$(2P_0)$	$(2P_{\pm 1}^{1/2})$	$(2P_{\pm 1}^{5/2})$
(i)	25.94	0.075	0.10	0.16	1.71	-0.7	0.34	0.42	0.18	0.35	0.21
(ii)	25.86	0.12	0.28	0.44	3.0	-1.08	1.42	1.77	0.75	2.31	0.89
(iii)	25.86	0.12	0.28	0.44	3.0	-1.08	1.37	1.65	0.51	1.86	0.8

$$g_A^\parallel = -6\kappa, \quad g_B^\parallel = 2[-\kappa - (\kappa+1)(3a^2-1)],$$

$$g_C^\parallel = 2[-\kappa - (\kappa+1)(3b^2-1)], \tag{31}$$

$$g_A^\perp = 0, \quad g_B^\perp = 2[-\sqrt{2}ab(3\kappa+1)+b^2],$$

$$g_C^\perp = 2[\sqrt{2}ab(3\kappa+1)+a^2], \tag{32}$$

and the coupling effective g values are

$$g_{BC}^\parallel = -6(\kappa+1)ab, \quad g_{BC}^\perp = \sqrt{2}(3\kappa+1)-4ab,$$

$$g_{AB}^\perp = -\sqrt{2}b(3\kappa+1)+2a, \quad g_{AC}^\perp = \sqrt{2}a(3\kappa+1)+2b. \tag{33}$$

Expressions for the orbital, $\hat{G}_{or}^{\parallel,\perp}$, anisotropic, $\hat{G}_{an}$, and coupling, $\hat{G}_{coup}^{\parallel,\perp}$, operators are given in Appendix B.

We assume in the following an additional condition on the weak external magnetic field, $\mu_B H \ll \Delta_1, \Delta_2$. This will allow us to the consider the effect of coupling to second order in perturbation theory. The parallel ($H_\parallel = H_z$) and perpendicular ($H_\perp = H_x$) magnetic field splits the S–state A, B, and C excitons into four lines with splitting energies,

$$\pm \frac{1}{2}(\mu_B H_{\parallel,\perp})(g_e^{\parallel,\perp} \pm g_{v,n}^{\parallel,\perp}), \tag{34}$$

where $g_{v,n}^\perp = g_v^\perp$ and independent of n, and $g_{v,n}^\parallel$ are the values of the effective parallel g factors of the hole involved in the corresponding exciton states:

$$g_{A,n}^\parallel = g_A^\parallel + \frac{96}{5n^2} \frac{m_0}{\mu_0} p_h^2 [(4a^2+\eta b^2)M_n(\Delta_1^0)$$

$$+ (4b^2 + \eta a^2)M_n(\Delta_2^0)], \tag{35}$$

$$g_{B,n}^\parallel = g_B^\parallel - \frac{2ab(1-\eta)p_h g_{BC}^\parallel}{n^2(\Delta_2^0-\Delta_1^0)} + \frac{96}{5n^2}\frac{m_0}{\mu_0}p_h^2[(4a^2-\eta b^2)$$

$$\times M_n(-\Delta_1^0) + \eta M_n(\Delta_2^0-\Delta_1^0)], \tag{36}$$

$$g_{C,n}^\parallel = g_C^\parallel - \frac{2ab(1-\eta)p_h g_{BC}^\parallel}{n^2(\Delta_1^0-\Delta_2^0)} + \frac{96}{5n^2}\frac{m_0}{\mu_0}$$

$$\times p_h^2[(4b^2-\eta a^2)M_n(-\Delta_2^0)+\eta M_n(\Delta_1^0-\Delta_2^0)], \tag{37}$$

where the functions $M_{n=1,2}$ are defined in Appendix A. The corrections $g_{v,n}^\parallel - g_v^\parallel$ come solely from the intersubband coupling and may depend on the external stress. For the model parameter sets (i), (ii), and (iii), the coupling corrections to the g factor of the A exciton ground state $g_{A,n=1}^\parallel - g_A^\parallel$ are 0.30, 1.22, and 1.18, respectively.

E. Fine structure of the A exciton and selection rules for optical transitions.

The symmetry of exciton states in wurtzite semiconductors and the selection rules for optical transitions have been studied in detail (see, for example, Refs. 49,22, and 26). For the A exciton, the ground $1S$ and all excited $n=2$ substates $2S$, $2P_0$, and $2P_{\pm1}$ have components of Γ_5 symmetry and are optically active for perpendicularly polarized light ($\mathbf{E}\perp c$). The excited $2P_{\pm1}$ states is the only one having a component with Γ_1 symmetry that is optically active for parallel polarized light ($\mathbf{E}\parallel c$). We note that both optically active components of the $2P_{\pm1}$ state, Γ_5 and Γ_1, arise from the $P_{\pm1}^{1/2}$ state defined in Sec. II C and are split from the dipole–forbidden states even in the absence of the electron–hole exchange interaction [which is not included in the exciton Hamiltonian of Eq. (1)].

We shall briefly describe the fine structure of the A-exciton ground state. At zero magnetic field the $1S$ state is split by the short–range exchange term into a dipole–forbidden Γ_6 state (with energy E_6) and a dipole–active Γ_5 state (with energy $E_5 = E_6 + \Delta_{56}$, where Δ_{56} is the energy of the short–range exchange interaction). For an exciton with wave vector parallel to the hexagonal axis $\mathbf{K}\parallel c$, both Γ_5 components are transverse Γ_{5T} states. For $\mathbf{K}\perp c$ one of the components is a longitudinal Γ_{5L} state and is shifted to higher energy $E_5 + \Delta_{LT}$ by the dipole-dipole interaction,[49,15] where Δ_{LT} is the longitudinal–transverse (LT) splitting of the exciton. The longitudinal exciton, Γ_{5L} and the forbidden exciton Γ_6 have no oscillator strength unless they are mixed with allowed states of the B exciton due to nonvanishing components of $\mathbf{K}\perp c$.[49,22] Further interaction of the transverse excitons Γ_{5T} with the radiation field leads to the formation of lower, Γ_{5T1}, and upper, Γ_{5T2}, transverse–polariton branches. Depending on the relaxation and scattering processes in the GaN layer, the excitation energy, and the excitation intensity, polaritons from both branches may contribute to the luminescence with energy peaks at about E_5 and $E_5 + \Delta_{LT}$.[50–53,17]

In a parallel external magnetic field $\mathbf{H}\parallel c$, the magnitude of the linear Zeeman splitting is proportional to $|g_e^\parallel - g_{A,1S}^\parallel|$ for Γ_5 and to $|g_e^\parallel + g_{A,1S}^\parallel|$ for Γ_6 states, respectively. A perpendicular magnetic field $\mathbf{H}\perp c$ mixes the Γ_5 and Γ_6 states through the term proportional to $g_e^\perp$. In addition, the diamagnetic interaction causes a shift of all states to higher energy. The energy levels of magnetoexcitons for different directions of $\mathbf{H}$ and $\mathbf{K}$ can be found, for example, in Refs. 54,55,23, and 56. A strong exciton–photon interaction in a magnetic field leads to the formation of magnetopolariton branches.[56] The calculated dependence of the allowed transition energies of the A excitons and excitons and polaritons on magnetic field is shown in Figs. 2(a)–2(e). For these calculations, we used model parameters of GaN, which are close to the values observed experimentally in our samples (see Sec. IV and Ref. 11): $\Delta_{56}=0.1$ meV, $\Delta_{LT}=1.0$ meV, and $g_e^\parallel = g_e^\perp = 2.0$. The values of the hole-parallel g factors were taken to be $g_{A,1S}^\parallel = 0.5$ in (a) and (c) and $g_{A,1S}^\parallel = 2.3$ in (b) and (d). The energies are given with respect to E_6 and the diamagnetic shifts $D_A^\parallel$ and $D_A^\perp$ are subtracted. For the case $\mathbf{K}\parallel c$ and $\mathbf{H}\parallel c$ [Figs. 2(a) and 2(b)] the projection of the total angular momentum on the c axis is a good quantum number. The allowed transitions for the right– and left–circularly polarized light are marked in Figs. 2(a) and 2(b) as σ^+ and σ^-, re-
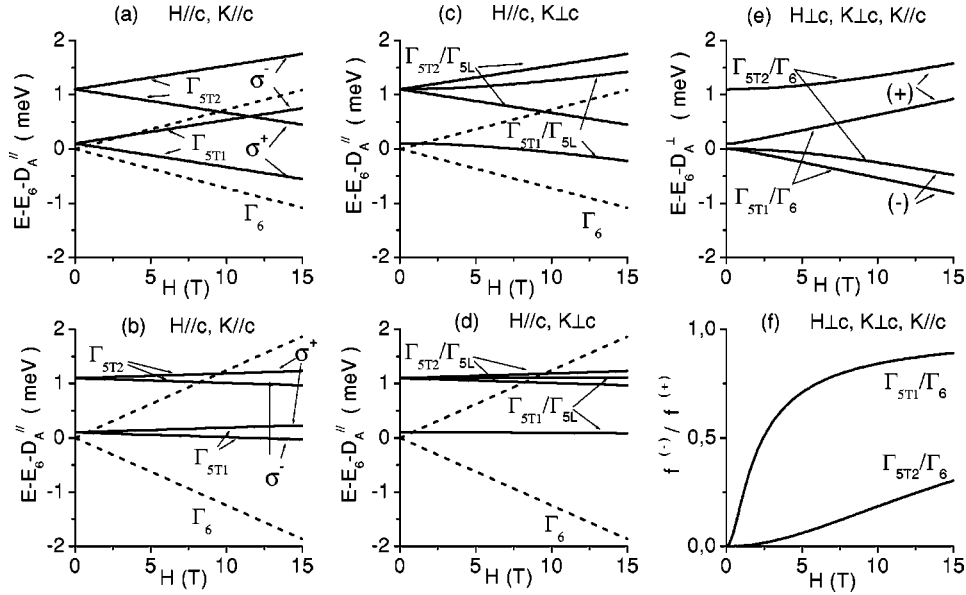
FIG. 2. Magnetic field dependence of the transition energies of the exciton polariton belonging to the *A* valence subband in low magnetic fields for various directions of the magnetic field **H** and wave vector of translation motion **K** relative to the hexagonal axis c: $\mathbf{H}\|c$, $\mathbf{K}\|c$ (a) and (b), $\mathbf{H}\|c$, $\mathbf{K}\perp c$ (c) and (d), and $\mathbf{H}\perp c$, $\mathbf{K}\|c$ or $\mathbf{K}\perp c$ (e). The field dependence of ratios of the oscillator strengths of the lower ($f^{(-)}$) and upper ($f^{(+)}$) mixed branches for perpendicularly polarized light for $\mathbf{H}\perp c$, $\mathbf{K}\|c$ or $\mathbf{K}\perp c$ is shown in (f). The GaN model parameters used in our calculations are $\Delta_{56}=0.1$ meV, $\Delta_{LT}=1.0$ meV, $g_e^{\|}=g_e^{\perp}=2.0$; $g_{A,1S}^{\|}=0.5$ in (a) and (c) and $g_{A,1S}^{\|}=2.3$ in (b) and (d).

spectively. For the case $\mathbf{K}\perp c$ and $\mathbf{H}\|c$ [Figs. 2(c) and 2(d)] all Γ_5 states are mixed Γ_{5L}/Γ_{5T} magnetopolariton states. The dipole–forbidden Γ_6 states are shown in Figs. 2(a)–2(d) as dashed lines. One can see that the field dependence and the magnitude of the Zeeman splitting of the optically allowed transitions in a parallel magnetic field depend dramatically on the value of the parallel hole effective g factor.

The field dependence of the optical transition energies for a perpendicular magnetic field $\mathbf{H}\perp c$ is the same as for $\mathbf{K}\|c$ and $\mathbf{K}\perp c$ [see Fig. 2(e)]. The resulting states are mixed Γ_5/Γ_6 magnetopolariton states (in the case $\mathbf{K}\perp c$, a mixed Γ_{5L}/Γ_6 exciton state, not shown in the figure, is also formed). For the case of perpendicularly polarized light, the oscillator strength of the mixed states will be determined by the contribution from the transverse polariton component, depending on the magnetic field, and the values of Δ_{56} and Δ_{LT}. We have calculated oscillator strengths f of all states allowed with perpendicularly polarized light as a function of magnetic field using the model parameters for GaN mentioned above. The ratios of the oscillator strengths $f^{(-)}$ and $f^{(+)}$ of the lower ($-$) and upper ($+$) branches of the mixed Γ_{5T1}/Γ_6 and Γ_{5T2}/Γ_6 states are shown in Fig. 2(f).

III. EXPERIMENT

The samples used for this study are high-quality GaN epilayers 300 μm (sample I) and 400 μm (sample II) thick, grown on (0001) sapphire by hydride vapor phase epitaxy (HVPE). Additional studies were performed using epitaxial laterally overgrown GaN layers (sample III) grown on (0001)sapphire by HVPE and metallo-organic vapor phase epitaxy. Details of the growth procedure were given in previous publications.[57,58] It is known, and we see it in our

work, that high-quality HVPE GaN typically has very intense and spectrally narrow emission lines at low temperature in the near-band-gap region.[2] Our HVPE samples were characterized with high spatial resolution, to 1 μm and 100 nm, by photo- and cathodoluminescence measurements,[59] respectively. From these studies, we know that the values of emission peak energies are sensitive to any inhomogeneous local strain present in the sample. Due to the narrow linewidth, typically less than 1 meV, even very small strain variations can cause peak shifts in the range of ± 0.1 meV. Despite the narrow linewidths and the high spectral resolution in our experiments, it is still not possible at present to give bulk reference energies with an accuracy better than 0.1 meV, due to the unavoidable variation of the position of the excitation spot in our experiments. Photoluminescence measurements were performed under continuous wave (cw) excitation at 325 nm using a HeCd laser for samples I and II and at 351 nm using an Ar laser for sample III. To distinguish between luminescence polarized parallel and perpendicular to the c axis, we detected the light from a side face of the epilayers (edge emission). The sample was mounted in an immersion cryostat at 2 K for zero-field experiments. For magnetoluminescence experiments in Faraday configuration ($\mathbf{k}\|\mathbf{H}$), a 15-T split-coil magnet was employed. To obtain PL spectral positions with as high an accuracy as possible, we made line shape fits to the measured spectra, using symmetric Gaussian or Voigt line shapes for the individual peaks. We always fit the complete free-exciton luminescence spectrum in order to obtain the highest possible accuracy in the energy positions. This simple analysis does not use any model of the polariton emission or of the physical processes involved. It serves only to determine observed peak positions to as high an accuracy as possible. On the other hand, it is
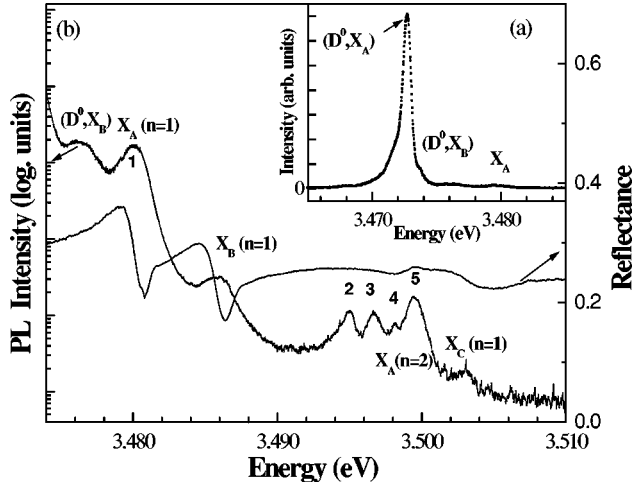
FIG. 3. Direct photoluminescence from exciton states in GaN using a (a) linear intensity scale and (b) a logarithmic scale. In (b) the corresponding reflection spectrum is shown (right axis). Sample II.

known that the direct excitonic emission line shape has very little asymmetry, since only polaritons with a vanishingly small wave vector **k** can leave the crystal as photons.[60] In addition, our GaN samples exhibit only a relatively small variation in reflection, and thus also transmission, from the sample surface in the excitonic range due to a comparatively high damping parameter, in the range of 0.7 meV.[61] Therefore, the influence of surface transmission can be neglected, and we can expect good agreement between measured spectra and the line shape fits.

IV. RESULTS

A. Overview of the unpolarized exciton PL spectrum in GaN

We first give an overview of the complete emission spectrum of GaN in the excitonic range. Figure 3 shows the unpolarized PL spectrum from the surface of a 400-μm-thick epilayer (sample II). On a linear scale, only the very strong and spectrally narrow donor-bound-exciton luminescence (D^0, X_A) at 3.4728 eV can be seen in Fig. 3(a). The linewidth of this emission is only 920 μeV. This allows us to observe a fine structure, labeled (D^0, X_B), on its high–energy shoulder at 3.476 eV, which we attribute to the emission of a donor–bound B exciton. However, detailed discussion of the nature of this luminescence line is beyond the scope of this paper. The direct emission X_A of the A exciton is also observed as a relatively weak line on the high–energy side of the bound–exciton spectrum.
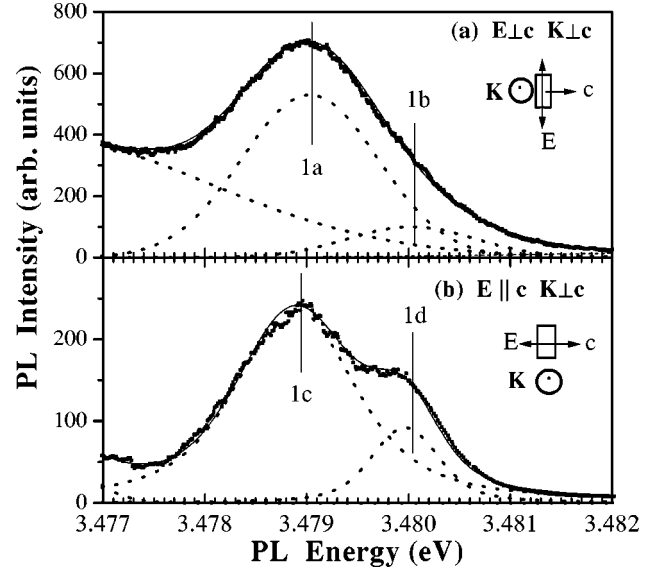

FIG. 4. Linearly polarized edge emission from the $n = 1$ state of the A exciton: (a) $\mathbf{E} \perp c$ and (b) $\mathbf{E} \| c$. Symbols represent experimental data, dashed lines fitted individual peaks; the solid line is the fit to the measured spectrum. Sample I.

On the logarithmic scale shown in Fig. 3(b), several narrow emission lines attributed to the A, B, and C excitons are observed. The reflection spectrum, recorded for the same sample with the same energy calibration, is shown for comparison. The splitting between the emission from the A exciton ground state (the line labeled 1) and the emission from the B and C exciton ground states, Δ_{AB} and Δ_{AC}, determined for samples I and II are given in Table III. The lines labeled from 2 to 5 in Fig. 3(b) are observed in all three samples. From comparison with our reflection measurements, only the lines labeled 4 and 5 are assigned to emission from the $n = 2$ excited states of the free A exciton. The origin of the lines labeled 2 and 3 cannot be well established. They may be attributed to the emission from an excited exciton bound to a ground state of a neutral donor $(D_0, X_{A, n=2})$, as was suggested by Scromme,[62] or to the donor–bound state of the C exciton.[24]

B. $n = 1$ ground state of the A exciton

1. Zero magnetic field

We now turn to a detailed investigation of the emission line, labeled 1, which belongs to the $n = 1$ state of the A exciton. To study its fine structure, we examine the PL in different geometries, i.e., for different directions of propagation and polarization of the emitted light. Figure 4 shows the

TABLE III. Exciton fine-structure splittings and effective g values in wurtzite GaN.

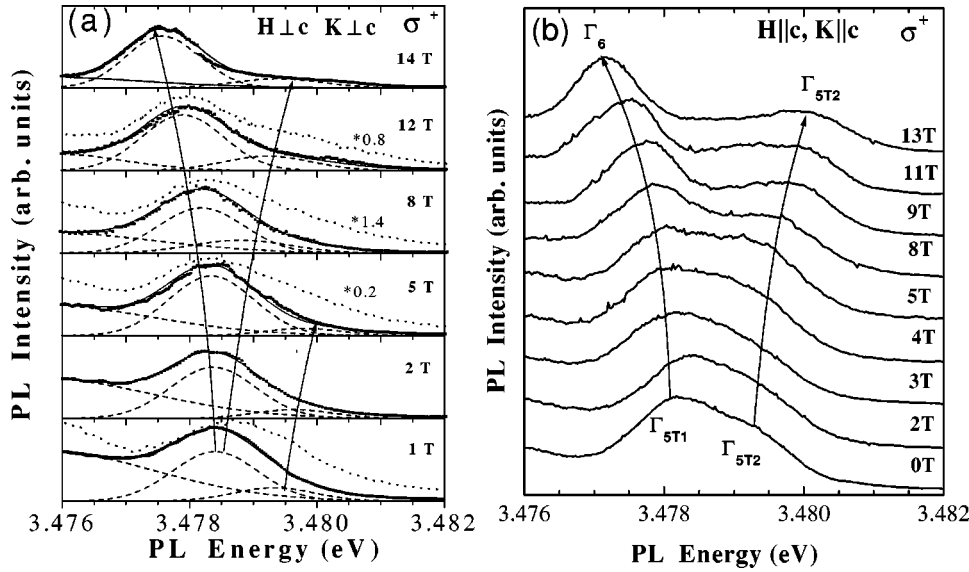|	Δ_{AB} (meV)	Δ_{AC} (meV)	Δ_{56} (meV)	Δ_{LT} (meV)	$E_A^0(2P_{\pm 1}) - E_A^0(1S)$ (meV)	$g_e^\perp$	$g_{A,1S}^\|$
Sample I	5.5±0.1	22.0±0.1	0.12±0.1	1.0±0.1	19.7±0.2	2.0±0.5	2.25±0.2
Sample II	6.0±0.1	22.2±0.1					

FIG. 5. Magnetoluminescence spectra from the state $n=1$ of the A exciton taken in Faraday configuration with circular polarization for perpendicular $\mathbf{H} \perp c$ (a) and parallel $\mathbf{H} \| c$ (b) directions of magnetic field relative to the hexagonal axis c. In (a) the results of line shape analysis are shown: symbols represent experimental data, dashed lines fitted individual peaks; the solid line is the fit to the measured spectrum. The dotted lines show the spectra taken at 25 K. The curves with arrows are guides to the eye. Sample I.

polarized low-temperature emission of photons from a side face of a free-standing 300-μm-thick sample (sample I) after interband excitation in the region of the $n=1$ state of the A exciton. In Fig. 4(a) the detected light is polarized perpendicular to the c axis, in Fig. 4(b) parallel to the c axis. The spectrum in Fig. 4(a) shows an emission line of approximately 3 meV half width, which is superimposed on the high–energy shoulder of the (D^0, X_B) line shown in Figs. 3(a) and 3(b). The emission from the B exciton is too weak and too far on the high–energy side to have an influence on the line shape. This emission line is asymmetrical with a broader high–energy shoulder. A line shape analysis performed, as described in Sec. III, for the whole spectrum (of which only a part is shown in this figure by dashed lines) reveals that the A-exciton emission in perpendicular polarization consists of two peaks, labeled $1a$ (at 3.4790 eV) and $1b$ (at 3.4800 eV). Although the high–energy peak $1b$ can be distinguished only with the help of the line shape analysis, its contribution must be included to obtain a good agreement with the measured spectrum (the sum of all fitted peaks shown by a solid line). We ascribe the peaks $1a$ and $1b$ to the emission from two transverse polariton branches $1S(\Gamma_{5T1})$ and $1S(\Gamma_{5T2})$.

The emission from the $n=1$ state of the A exciton with parallel polarization is expected to vanish.[22] However, as Fig. 4(b) shows, rather strong emission is observed with an intensity about one-third of that for perpendicular polarization. Two peaks labeled $1c$ (at 3.4789 eV) and $1d$ (at 3.4800 eV) can be clearly distinguished. We ascribe peak $1d$, observed at the same energy as peak $1b$ with perpendicular polarization, to the emission from the longitudinal exciton states $1S(\Gamma_{5L})$. Peak $1c$, observed in parallel polarization, is 120 μeV below peak $1a$ [$1S(\Gamma_{5T1})$] observed in perpendicular polarization. We attribute peak $1c$ to the dipole–forbidden state $1S\Gamma_6$, which gives a value of the spin–exchange splitting as $\Delta_{56} = 0.12 \pm 0.1$ meV. The distance between the energy positions of the $1S(\Gamma_{5T1})$ state [peak $1a$ in Fig. 4(a)] and the $1S(\Gamma_{5T2})/1S(\Gamma_{5L})$ states [peaks $1b$ and $1d$ in Figs. 4(a) and (b)] gives us an approximate value of

the longitudinal–transverse splitting as $\Delta_{LT} = 1.0 \pm 0.1$ meV.

2. External magnetic field

The emission of the $n=1$ state of the A exciton in magnetic fields perpendicular and parallel to the c axis is shown in Figs. 5(a) and 5(b), respectively. Both series were taken in the Faraday configuration $\mathbf{K} \| \mathbf{H}$ and detecting circularly polarized light. We observe a systematic blue shift, of 210 μeV, of the whole spectrum taken from the surface compared to the side face emission, and ascribe this to a different local strain at the surface than at the side face of the sample. The peak positions in the edge geometry at zero field are slightly different from those shown in Fig. 4 due to local strain variations.

We first discuss the dependence of the transition energies for a perpendicular magnetic field in edge geometry: $\mathbf{K} \perp c$, $\mathbf{H} \perp c$. Line shape fits of the observed peaks are shown by dashed lines in Fig. 5(a). Also included in this figure are spectra taken at 25 K (dotted lines) for magnetic fields of 1, 5, 8, and 12 T. At low magnetic fields the dominant emission is from the upper split mixed branch $1S(\Gamma_{5T1}/\Gamma_6^{(+)})$. With increasing magnetic field the oscillator strength of the lower split $1S(\Gamma_{5T1}/\Gamma_6^{(-)})$ branch increases (see Fig. 2) and the low-energy peak consists of unresolved emission from both $1S(\Gamma_{5T1}/\Gamma_6)$ mixed states. Starting from a magnetic field of about 5 T, the transverse Γ_{5T1} component gives equal contributions to the lower and upper split $1S(\Gamma_{5T1}/\Gamma_6)$ mixed branches. The corresponding emission peak moves to lower energies with increasing magnetic field because relaxation processes result in a larger population of the lower state. For magnetic fields larger than 8 T, emission from the upper split $1S(\Gamma_{5T1}/\Gamma_6^{(+)})$ branch can be detected by line shape analysis at almost exactly the same energy where the corresponding shoulder appears in the spectra taken at 25 K. One can see that, with increasing temperature, the emission from the upper split state increases, which can be understand by an increase of its population. The emission from the upper
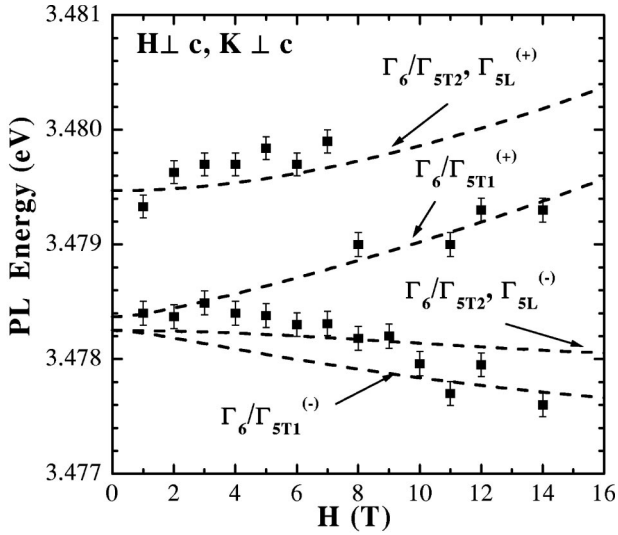
FIG. 6. Magnetic field dependence of the energy peaks of the edge emission from the $n=1$ state of the A exciton for magnetic field and wave vector perpendicular to hexagonal axis ($\mathbf{K}\perp c$, $\mathbf{H}\perp c$). Sample I.

$1S(\Gamma_{5T2}/\Gamma_6)$ polariton and the $1S(\Gamma_{5L}/\Gamma_6)$ exciton states is weak and, at low temperatures, can only be observed up to 7 T. The corresponding peak shifts to higher energies with increasing magnetic field. The magnetic field dependence of the energy peak positions obtained by the line shape fits is shown in Fig. 6. The values of the spin–exchange and LT splittings used for fitting the data in Fig. 6 (the dashed curves are calculated using expressions given in Ref. 54) are $\Delta_{56}=0.12$ meV and $\Delta_{LT}=1.1$ meV; the value used for the electron perpendicular g factor is $g_e^\perp=2.0\pm0.05$.

The emission spectrum of right-circularly polarized light from the surface for a parallel magnetic field ($\mathbf{K}\|c,\mathbf{H}\|c$) is shown in Fig. 5(b). For zero magnetic field two emission peaks, from the two polariton branches $1S(\Gamma_{5T1})$ and $1S(\Gamma_{5T2})$, are clearly seen with an energy separation of about $\Delta_{LT}=1.1$ meV. Applying the parallel magnetic field leads to a Zeeman splitting not only of the twofold degenerate $1S(\Gamma_{5T1})$ and $1S(\Gamma_{5T2})$ polariton states but also of the dipole–forbidden $1S(\Gamma_6)$ exciton state shown in Figs. 2(a) and 2(b). For σ^+ polarization a magnetic field shifts the dominant lower-energy peak to lower energies and the high-energy peak to higher energies [see Fig. 5(b)]. The same behavior of the magnetic field was observed for σ^--polarized emission. Thus we conclude that we are observing emission from the forbidden $1S(\Gamma_6)$ state, which is shifted to energies lower than the $1S(\Gamma_{5T1})$ state in large magnetic fields [corresponding to the situation in Fig. 2(b)]. The Zeeman splitting for both $1S(\Gamma_{5T1})$ and $1S(\Gamma_{5T2})$ states is almost compensated due to the near equality of the electron and hole effective g factors in parallel magnetic fields, and cannot be detected in the difference between the σ^+ and σ^--polarized components. The corresponding Zeeman splitting for the $1S(\Gamma_6)$ state is, in contrast, large. We will discuss, in Sec. VI, the possible reasons for the observation of the emission from the dipole–forbidden Γ_6 state and its large oscillator strength.
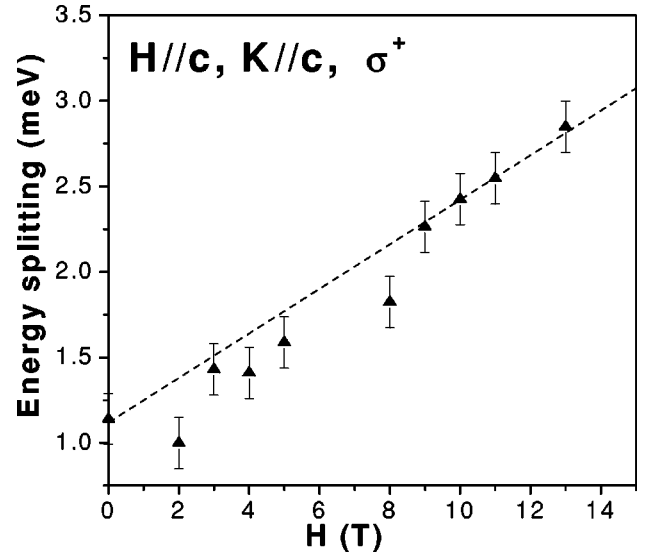

FIG. 7. Magnetic field dependence of the splitting between uppermost and lowest peaks of the surface emission from the $n=1$ state of the A exciton measured with σ^+ polarization for magnetic field and wave vector parallel to the hexagonal axis ($\mathbf{K}\|c$, $\mathbf{H}\|c$). Sample I.

The magnetic field dependence of the observed splitting between the uppermost and the lowest σ^+ polarized PL peaks is shown in Fig. 7. We suggest that in large magnetic fields these emission peaks arise from the raised Γ_{5T2} state and the lowered Γ_6 state, respectively, with energy splitting between them given by $\Delta_{56}+\Delta_{LT}+2g_{A,1S}(\mu_B H)$ (the dashed line). From the splitting in large magnetic fields the
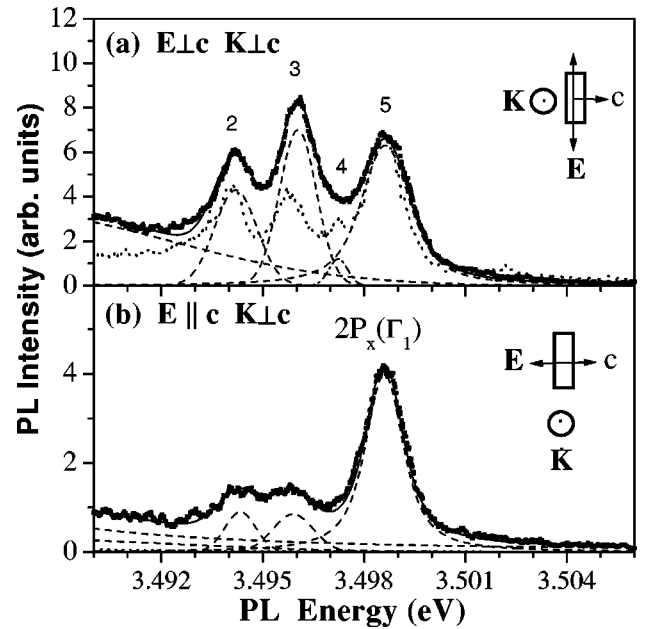
FIG. 8. Linearly polarized high energy edge emission: (a) $\mathbf{E}\perp c$ and (b)$\mathbf{E}\|c$. Symbols represent experimental data, dashed lines fitted individual peaks; the solid line is the fit to the measured spectrum. Sample I. The dotted line in (a) shows the redshifted and rescaled unpolarized PL for sample II.

effective parallel g factor of the hole involved in the $1S$ state of the A exciton is estimated to be $g_{A,1S}=2.25\pm0.2$. In smaller magnetic fields the low-energy peaks are composed of emission from the $1S(\Gamma_{5T1})$ and $1S(\Gamma_6)$ states.

C. $n=2$ state of the A exciton

We now turn to the investigation of the emission lines labeled 2–5 in Fig. 3. In Fig. 8, the low-temperature PL of sample I polarized perpendicular (a) and parallel (b) to the c axis is shown in the region of the $n=2$ state of the A exciton. For comparison the unpolarized PL for sample II is also shown as a dotted line in Fig. 8(a). We have redshifted the unpolarized spectrum in this figure to lower energies by 850 μeV and rescaled it. The emission from two lower-energy peaks 2 and 3 at 3.4942 eV and 3.4961 eV is strong for perpendicular and weak for parallel polarization. The intensity of the high-energy peak 5 is only weakly dependent on the polarization. This emission line is centered at 3.4986 eV for both polarizations but is narrower for parallel polarization. We conclude that peak 5 is a superposition of two or more degenerate Γ_5 and Γ_1 states that are allowed for the perpendicular and parallel polarization, respectively. The weak line 4 at 3.4972 eV, clearly visible in the unpolarized spectrum of sample II, is hidden in the polarized spectra of sample I due to the increased width of lines 3 and 5. However, we see an asymmetric broadening on the low–energy shoulder of line 5. In the line shape analysis for the perpendicular polarized spectrum of sample I it was necessary to include an additional peak at line 4 to obtain a good fit. However, its weakness makes it difficult to make an unambiguous statement about its polarization properties.

From the position of line 5 in parallel polarization, the energy of the $2P_{\pm1}(\Gamma_1)$ state can be determined. The distance between the $1S$ and $2P_{\pm1}$ states of the A exciton obtained for sample I is 19.7 ± 0.2 meV. Two different conclusions are possible concerning the splitting of the $n=2$ state of the A exciton at zero magnetic field. Either the single broad strong line 5 at 3.4986 eV (with width about 1.5 meV for the perpendicular polarization) corresponds to the $n=2$ state of the free A exciton with unresolved splittings, or the weak line 4 at 3.4972 eV originates from the emission of the $2P_0$ or $2S$ state of the A exciton, and the strong line 5 corresponds to the unresolved emission from other $n=2$ sublevels. The energy splitting between peaks 4 and 5 for sample I is 1.3 ± 0.1 meV.

We have studied the magnetic field dependence of the lines 2–5 in parallel and perpendicular magnetic fields in Faraday configuration. For parallel fields, we have not detected any additional splitting. All lines are broadened and shifted to higher energy with increasing magnetic field. For perpendicular magnetic fields the emission peaks show a linear Zeeman splitting and also a diamagnetic shift to higher energy with increasing magnetic field. However, we were not able to make an unambiguous identification of the lines observed.

V. COMPARISON OF THEORY WITH EXPERIMENTAL DATA

A. A-exciton effective Rydberg number and polaron corrections

We turn now to the determination of the value of the A exciton effective Rydberg number and the ground-state binding energy. Using the isotropic hydrogenlike model, we can estimate the ground-state binding energy and the A-exciton effective Rydberg number from the observed distance between the $n=1$ and $n=2$ states: $E_{A,1S}^{bind}=R_A=\frac{4}{3}(E_{A,n=2}^0-E_{A,n=1}^0)=26.3\pm0.3$ meV. One can see from Table II that the total (anisotropy plus intersubband coupling) corrections to the ground and excited states of the A exciton depend strongly on the value of the hole effective mass anisotropy, which is not known at this time. Using the $2P_{\pm1}^{1/2}$ state as the reference energy for the $n=2$ state can lead to an error in the binding energy of the A-exciton ground state of about $\pm1\%$ and in the exciton effective Rydberg number of about $\pm7\%$. Therefore, we estimate the A-exciton effective Rydberg number as $R_A=25.5\pm1.1$ meV and the ground-state binding energy as $E_{A,1S}^{bind}=26.2\pm0.4$ meV. The maximum splitting between the lowest $2P_0$ state and the uppermost optically active $2P_{\pm1}^{1/2}$ state of the A exciton is estimated to be 0.5 meV.

We have been using static dielectric constants for the electron–hole Coulomb interaction in Eq. (1). Now, the value of the A exciton effective Rydberg estimated above is associated with electron–polaron and hole–polaron effective masses. However, the difference between the static and the high-frequency dielectric constants in GaN is known to be very large[32,33] and the effects associated with a spatially dependent screening of the electron–hole interaction[34,35] may be significant. In order to evaluate these "polaron" corrections for the exciton levels in GaN, we consider now the effect of two model potentials for the electron–hole effective Coulomb interaction derived for semiconductors with a simple isotropic band structure in Refs. 34 and 35. These isotropic potentials have been found to be a good approximation when compared with the similar fully anisotropic potentials derived for anisotropic semiconductors with simple bands.[38,36] As the high-frequency dielectric constant ε_∞ is known to be isotropic in GaN,[32,33] we will continue to use the parameter $\eta=\varepsilon_0^\perp/\varepsilon_0^\parallel$ when taking into account the anisotropy of the Coulomb part of the electron–hole interaction.

For simplicity, we shall take the electron, $m_e=m_e^\parallel=m_e^\perp$, and electron–polaron, m_e^*, effective masses in GaN to be isotropic and related by $m_e^*=m_e(1+\alpha_e/6)$, where $\alpha_e=\sqrt{m_e e^4/2\hbar^2\varepsilon^{*2}E_{lo}}$ is the electron Fröhlich interaction constant and $1/\varepsilon^*=(1/\varepsilon_\infty-1/\varepsilon_0)$. The hole–polaron effective masses in the A, B, and C valence subbands, $m_v^{*\parallel,\perp}$, can be obtained from Eqs. (10)–(12) using the renormalized effective Luttinger parameters $\gamma_1^*=\gamma_1/(1+\alpha_h/6)$ and $\gamma^*=\gamma/(1+\alpha_h/6)$. The hole interaction constant is given by $\alpha_h=\sqrt{m_h e^4/2\hbar^2\varepsilon^{*2}E_{lo}}$, where the mass $m_h=m_0/\gamma_1$ is the hole effective mass averaged over the three directions in $\mathbf{k}$ space. The polaron self-energy $E_{pol}=(\alpha_e+\alpha_h)E_{lo}$ is the same for all exciton states, so that the experimentally rel-

evant value of the energy band gap is $E_g = E_{g,\infty} - E_{pol}$, and the spacing between the valence subbands Δ_1 and Δ_2 remains unchanged. We see from Eqs. (10)–(12) that the hole polaron masses are related to the "bare" masses by $m_v^{*\|,\perp} = m_v^{\|,\perp}(1 + \alpha_h/6)$ ($v = A, B, C$) just as for the electron effective masses in the Fröhlich model.

We shall use the averaged parameters defined above in the isotropic Haken and Pollmann–Büttner effective potentials. The Haken model describes two interacting polarons, each with a radius much smaller than the exciton effective radius, and expresses the effective potential for the electron–hole Coulomb interaction as[34]

$$V_H(r) = -\frac{e^2}{\varepsilon_0 r} + V_H^*(r),$$

$$V_H^*(r) = -\frac{e^2}{2\varepsilon^* r}\left[\exp\left(-\frac{r}{l_e}\right) + \exp\left(-\frac{r}{l_h}\right)\right]. \quad (38)$$

Here $l_{e,h} = \sqrt{\hbar^2/2m_{e,h}E_{lo}}$ are the electron– and hole–polaron radii determined using "bare" band electron and hole effective masses. The polaron effective mass parameters must be used in the kinetic energy parts of the Hamiltonians. One can see that the Coulomb potential with a static dielectric constant is the limiting case of the Haken potential for $l_e, l_h \to 0$.

The model proposed by Pollmann and Büttner[35] takes into account the correlation between electron and hole polarons, and leads to corrections to the Haken potential. The resulting electron–hole interaction potential is

$$V_{PB}(r) = -\frac{e^2}{\varepsilon_0 r} + V_{PB}^*(r),$$

$$V_{PB}^*(r) = -\frac{e^2}{\varepsilon^* r}\frac{1}{\Delta m}\left[m_h \exp\left(-\frac{r}{l_h}\right) - m_e \exp\left(-\frac{r}{l_e}\right)\right], \quad (39)$$

with $\Delta m = m_h - m_e$. This potential was derived assuming $a_{ex} \gg l_{e,h}$, where $a_{ex} \approx a_v = \hbar^2 \varepsilon_0/e^2 \mu_v$ ($v = A, B, C$) are the effective radii of the respective exciton states. In GaN this condition is valid not only for the excited states but also for the ground exciton state. According to Pollmann and Büttner,[35] "bare" band electron and hole masses must be used in the kinetic energy terms of the Hamiltonians.

To calculate the exciton energy structure in zero magnetic field with the Haken or Pollmann-Büttner model, we need to replace the static Coulomb potential in the isotropic uncoupled Hamiltonian $\hat{H}_0$ with $V_H(r)$ or $V_{PB}(r)$. Exact solutions for this problem, however, do not exist. Therefore, as a zeroth approximation we use the wave functions (17) obtained for the Hamiltonian $\hat{H}_0$ using the static Coulomb potential and consider the Haken or Pollmann–Bütther correction potentials $V_H^*(r)$ and $V_{PB}^*(r)$ as a perturbation. The exciton energy structure in zero magnetic field is then described by Eq. (18) with additional terms $\Delta E_{v,n,l,m}^*$ ($v = A, B, C$) containing the polaron corrections added to the exciton binding energies of Eq. (19). We have calculated the

Haken and Pollmann-Büttner polaron corrections $\Delta E_{v,n,l,m}^*$ to second order in perturbation theory, using the model parameters of GaN and values of the dielectric constants from Refs. 32 and 33. The Haken polaron corrections are $\sim 0.33R_v$ for the $1S$ states of the A, B, and C excitons and $\sim 0.12R_v$ for the $2S$ states. The corresponding corrections for the Pollmann–Büttner model are about $0.11R_v$ and $0.04R_v$, respectively. The polaron corrections for the $2P$ states, as well as for the $n \geq 3$ excited states are negligible. Thus we may conclude that taking polaron corrections into account is extremely important in determining the exciton effective Rydberg number and the ground-state binding energy in GaN.

The zero-field exciton energy structure in GaN, taking into account anisotropy, coupling and polaron corrections, is shown in Fig. 1(d). We see that the coupling and polaron corrections in GaN affect the order of the $n = 2$ excited states, making the $2S$ state the lowest. The maximum splitting between the $2S$ state and the uppermost optically active $2P_{\pm 1}^{1/2}$ state of the A exciton can be as large as 1.2 meV or 0.9 meV, using the Haken and Pollmann–Büttner polaron models, respectively. The net effect of a weak external magnetic field and the exciton–LO-phonon interaction can be determined neglecting the coupling between the magnetic and phonon fields.[37] In this case, there are no "polaron" corrections to the linear Zeeman effect and the expressions for the hole-parallel effective g values obtained in Sec. II D must be used with respective "band" or "polaron" values of the electron and hole effective masses.

B. Effective masses and the magnetic Luttinger parameter in GaN

In this section we determine the effective Luttinger parameters and the magnetic constant in wurtzite GaN by fitting the experimental data (see Table III) using three models of the electron–hole Coulomb interaction: static Coulomb, Haken, and Pollmann–Büttner models. To minimize the number of fitting parameters, we keep fixed the value of the electron–polaron effective mass $m_e^* = 0.22m_0$.[6,43] Two sets of dielectric constants known for GaN have been used: (a) $\varepsilon_0^{\|} = 10.1$, $\varepsilon_0^{\perp} = 9.28$, and $\varepsilon_\infty = 5.29$ (Ref. 33) and (b) $\varepsilon_0^{\|} = 10.4$, $\varepsilon_0^{\perp} = 9.5$, and $\varepsilon_\infty = 5.35$ (Ref. 32) For both sets, a value of the "bare" electron mass $m_e = 0.204m_0$ is obtained with the Fröhlich interaction constant $\alpha_e \approx 0.47$. The values of the spin–orbit interaction constants and crystal field energy must be varied together with the effective Luttinger parameters in order to fit the experimental splittings between the ground states of the A, B, and C excitons. If one neglects the difference between the A, B, and C exciton binding energies, the splittings $\Delta_{AB} = \Delta_1$ and $\Delta_{AC} = \Delta_2$ can be fit to within experimental error, with the values $\Delta_{so}^{\|} = 18.5 \pm 0.2$ meV, $\Delta_{so}^{\perp} = 17.1 \pm 0.2$ meV and $\Delta_{cr} = 9.1 \pm 0.1$ meV, $\Delta_{cr} = 9.7 \pm 0.1$ meV for samples I and II, respectively. Estimates show that varying the spin–orbit and crystal field energy parameters within this range does not influence the structure of the A-exciton energy levels very much. To simplify the fitting procedure, we choose the val-
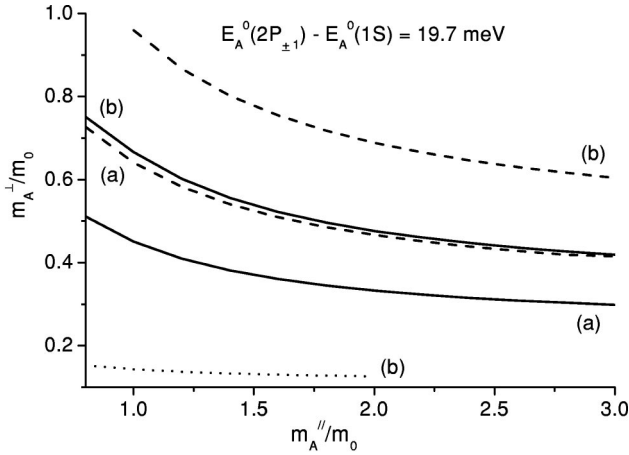
FIG. 9. Correlated pairs of values of the bare perpendicular and parallel hole effective mass in the A valence subband, $m_A^\perp$ and $m_A^\parallel$ that fit the splitting of the $1S$ and $2P_{\pm 1}$ A-exciton states, $E_A^0(2P_{\pm 1}) - E_A^0(1S) = 19.7$ meV, using the static Coulomb potential (dashed curves), the Haken (dotted curve), and Pollmann-Büttner models (solid curves). Cases (a) and (b) are for the two respective sets of dielectric constants described in the text.

ues $\Delta_{cr} = 9.1$ meV, $\Delta_{so}^\parallel = 18.5$ meV, and $\Delta_{so}^\perp = 17.1$ meV and focus, at first, on describing the A-exciton energy structure.

Thus, we fit the effective Luttinger parameters γ_1 and γ for the "bare" valence band [which, we see from Eq. (10), is equivalent to fitting the parallel and perpendicular "bare" hole effective masses in the A valence subband] to the splitting between the $1S$ and the $2P_{\pm 1}$ states of the A exciton, $E_A^0(2P_{\pm 1}) - E_A^0(1S) = 19.7$ meV. The resulting parameters are presented as lines of constant energy splitting in the space of the A valence subband hole effective masses $m_A^\parallel$ and $m_A^\perp$ in Fig. 9. These lines establish a correspondence between the parallel and perpendicular hole masses in the A valence subband for each polaron model for the particular dielectric constants chosen. The parameters obtained then allow us to calculate the entire exciton energy level structure in zero magnetic field.

To determine the value of the magnetic Luttinger constant κ, we use the well-known relationship between κ and the Luttinger γ parameters for a "bare" band:[63] $\kappa = (-2 - \gamma_1 + 5\gamma)/3$. This allows us to calculate the values of free-hole effective g factors in the valence subbands and the hole g factors in the exciton states. In Fig. 10 the calculated dependence of the parallel effective g factor of the hole involved in the $1S$ state of the A exciton, $g_{A,1S}^\parallel$, on the "bare" hole parallel mass $m_A^\parallel$ is shown. A comparison with the experimental value $g_{A,1S}^\parallel = 2.25 \pm 0.2$ shows that the most appropriate description of the data is obtained with the Pollmann-Büttner polaron model using set (a) of the dielectric constants. Using set (b) leads to unphysically large values of the hole-parallel mass in the A valence subband, as does also the static Coulomb potential using either set (a) or (b). The Haken polaron model predicts a value of the hole-parallel g factor smaller than 1.4, which is not consistent with experimental data.[64]
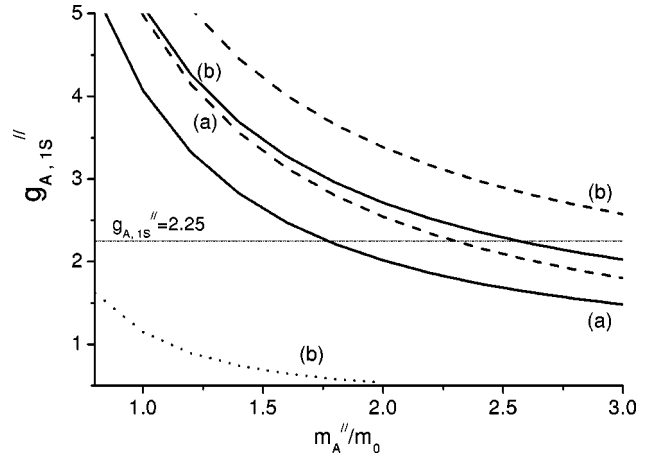

FIG. 10. The dependence of the hole parallel effective g factors in the A-exciton $1S$ state, $g_{A,1S}^\parallel$, on the bare hole parallel effective mass in the A subband, $m_A^\parallel$, calculated with the static Coulomb potential (dashed curves), the Haken (dotted curve), and Pollmann-Büttner models (solid curves). Cases (a) and (b) are for the two sets of dielectric constants described in the text, respectively.

We now focus on the implications of the Pollmann-Büttner polaron model and the dielectric constants of set (a). At this stage, we fit the spin-orbit and crystal field energy parameters to the experimentally observed splittings $\Delta_{AB} = 5.5$ meV and $\Delta_{AC} = 22.0$ meV of sample I. The result is $\Delta_{cr} = 10.3$ meV, $\Delta_{so}^\parallel = 19.4$ meV, and $\Delta_{so}^\perp = 19.2$ meV, which gives valence band splittings of $\Delta_1 = 5.6$ meV and $\Delta_2 = 24.1$ meV. From the measured g factor 2.25 ± 0.2 and the measured splitting between the $1S$ and $2P_{\pm 1}$ states, 19.7 ± 0.2 meV, we find the hole masses for the "bare" A subband as $m_A^\parallel = (1.76 \pm 0.3)m_0$ and $m_A^\perp = (0.35 \pm 0.025)m_0$. The Luttinger γ parameters for the "bare" band, then, are $\gamma_1 = 2.1$ and $\gamma = 0.77$ and the magnetic Luttinger constant is $\kappa = -0.09$. Values of the polaron effective Luttinger parameters $\gamma_1^* = 1.87$ and $\gamma^* = 0.68$ can be now obtained using the hole Fröhlich interaction constant $\alpha_h \approx 0.72$. The values of the "bare" band and polaron effective masses for the A, B, and C valence subbands are given in Table IV, together with the corresponding A, B, and C exciton effective Rydberg numbers. The binding energies of the A, B, and C excitons as well as the energies of the $n = 2$ sublevels relative to the ground state of the A exciton (calculated using the Pollmann-Büttner model with "bare" band effective masses) are given in Table V. We see that the total correction to the exciton ground-state binding energy, arising from the effects of anisotropy, intersubband coupling and optical phonon interactions, is about 20%. The effective parallel g factor of the hole in the A-exciton $1S$ state, $g_{A,1S}^\parallel = 2.25$, differs significantly from the hole effective parallel g factor for the uncoupled A subband $g_A^\parallel = -6\kappa = 0.54$ due to the effect of the intersubband coupling.

VI. DISCUSSION AND CONCLUSION

In this section we discuss our results in the context of the existing literature on GaN. In Sec. IV B we interpreted the

TABLE IV. Hole effective masses and exciton effective Rydberg numbers in wurtzite GaN.

	$\dfrac{m_A^{\parallel}}{m_0}$	$\dfrac{m_A^{\perp}}{m_0}$	$\dfrac{m_B^{\parallel}}{m_0}$	$\dfrac{m_B^{\perp}}{m_0}$	$\dfrac{m_C^{\parallel}}{m_0}$	$\dfrac{m_C^{\perp}}{m_0}$	$\dfrac{m_h}{m_0}$	R_A (meV)	R_B (meV)	R_C (meV)	R_0 (meV)
"Bare"	1.76	0.349	0.419	0.512	0.299	0.676	0.476	21.15	21.31	21.39	21.28
Polaron	1.972	0.391	0.469	0.579	0.335	0.757	0.534	23.08	23.24	23.33	23.22

observed fine structure of the $n=1$ state of the A exciton as caused by the exchange interaction and the polariton effect. The surface luminescence from the lower and upper polariton branches in GaN have been observed by Gil *et al.*[53] and by Stepniewski *et al.*[17]. The value of the spin–exchange splitting between the $1S(\Gamma_6)$ and $1S(\Gamma_{5T1})$ states, 120 μeV, was obtained directly from the energy shift between the perpendicularly and parallel polarized PL peaks and confirmed by fitting the magnetoluminescence data. It is smaller than the value reported in Ref. 21 for wurtzite GaN grown onto a–plane sapphire (0.6 meV) and also the value obtained in Ref. 12 by fitting the magnetoreflectance (0.9 meV). The value of the LT splitting of the A exciton, 1.0 ±0.1 meV, is in good agreement with those reported in Ref. 61 (0.97 meV) and Ref. 17 (0.9 meV) from the reflectance measurements.

Our magnetoluminescence measurements have confirmed the interpretation of the zero-field fine structure of the A-exciton–polariton ground state. The value of the perpendicular conduction band g factor, $g_e^{\perp}=2.0\pm0.05$, is in good agreement with the values $g_e^{\parallel}=1.9510$ and $g_e^{\perp}=1.9483$ obtained from electron spin resonance measurements by Carlos *et al.*[65] For a parallel magnetic field $\mathbf{H}\|c,\mathbf{K}\|\mathbf{H}$, we observed a zero Zeeman splitting of the optically active $1S(\Gamma_5)$ polariton states. This indicates the closeness of the electron and hole effective parallel g factors, in good agreement with results reported in Refs. 62,12,13, and 66. From the splitting between the upper transverse polariton $1S(\Gamma_{5T2})$ and the lower forbidden $1S(\Gamma_6)$ exciton in large magnetic fields, we determined the parallel effective g factor of the hole from the A valence subband involved in the $1S$ exciton state as $g_{A,1S}^{\parallel}=2.25\pm0.2.$[64] This value is in a good agreement with the value $g_{A,1S}^{\parallel}=2.3$ determined in Ref. 13 from the splitting between the right- and left-polarized Γ_5 components of both the upper and lower polariton branches. We note, however, that the resulting value of the magnetic Luttinger constant, $\kappa=-0.09$, is different from those obtained in Refs. 12 and 13 with the help of the expression $\kappa=-g_{A,1S}^{\parallel}/6$. This is because the hole effective parallel g factor in exciton states differs significantly from the A valence subband free-hole g

factor, $g_A^{\parallel}=0.54$, due to the coupling of the excitonic states in different valence subbands.

Surface emission from the dipole–forbidden Γ_6 state in a parallel magnetic field was previously observed in Ref. 23 for CdS and explained by additional scattering processes between the Γ_6 and Γ_5 states caused by impurities, phonons, internal stress, etc. It was noted[23] that thermalization favors a high population of the low–energy Γ_6 component in large magnetic fields, which is shifted to an energy below the Γ_{5T1} state. In GaN, the Zeeman splitting of the forbidden Γ_6 state is even larger than in CdS.[23] In magnetic fields $H>8$ T, we observed only weak emission from the lowest Γ_{5T1} polariton branch and a strong emission from the forbidden Γ_6 state, which was not observed in Refs. 62 and 13. We conclude, therefore, that the relaxation processes in our sample are faster than the radiative process connected with the converting of the Γ_{5T1} polaritons into photons. We also note that, in contrast to the situation reported in Ref. 13, we have observed the dominant emission in zero magnetic field from the lower polariton branch Γ_{5T1}, confirming the efficiency of the energy relaxation processes in our sample.

Unpolarized direct PL in the region of the $n=2$ state of the A excitons in GaN was previously reported by several authors, including our group.[2,62,20,67,24,25,16] The situation in this spectral range is complicated because excited states of both the A and B excitons, as well as emission from donor–bound complexes, can appear here, and interpretations of the observed emission lines given so far vary considerably. A proper determination of the distance between the $n=1$ state and the $n=2$ sublevels, however, is necessary for a proper evaluation of the exciton effective Rydberg value. We have used polarized measurements to identify the parallel polarized emission from the $2P_{\pm1}(\Gamma_1)$ state and the $1S(\Gamma_6)$ states in the same spectrum and evaluated the energy difference between the $1S$ and $2P_{\pm1}$ states of the A exciton as 19.7 ± 0.2 meV. Previous measurements of the $2P$ state in a two–phonon absorption (TPA) experiment[9] do not measure this quantity, because the TPA is insensitive to the $n=1$ exciton state.

We have determined the binding energy of the ground n

TABLE V. Binding energies of the A, B, and C exciton ground states and the energy levels of the A exciton in wurtzite GaN. The energies of the $n=2$ sublevels are given relative to the ground $n=1$ state.

$E_{A,n=1}^{bind}$ (meV)	$E_{B,n=1}^{bind}$ (meV)	$E_{C,n=1}^{bind}$ (meV)	$E_{A,n=2}(2S)$ (meV)	$E_{A,n=2}(2P_0)$ (meV)	$E_{A,n=2}(2P_{\pm1}^{1/2})$ (meV)	$E_{A,n=2}(2P_{\pm1}^{5/2})$ (meV)
25.21	25.3	27.3	18.84	19.11	19.7	19.97

=1 state of the A exciton as 25.2 ± 0.3 meV, which is comparable to the values reported by other groups.[24,9] The value of the exciton effective Rydberg number $R_A = 21.1 \pm 0.3$ meV, however, differs from the ground-state binding energy by about 25%. The major source of this discrepancy lies in the large polaron corrections to the $1S$ and $2S$ exciton energies. We estimated these corrections, using the Pollmann–Büttner polaron model developed for semiconductors with a simple band structure,[35] and do not claim to give an accurate description of polaron effects in wurtzite GaN. In addition, our treatment of the correction potential as a perturbation is not as accurate as our accounting of the anisotropic and coupling effects for bare exciton states. Nevertheless, we were able to draw some conclusions about the importance of polaron corrections in wurtzite GaN both for the determination of the exciton effective Rydberg numbers and for describing the excited $n = 2$ exciton-state splitting.

We have found that the order of the $n = 2$ sublevels and their energy splitting in wurtzite GaN are strongly affected by the intersubband coupling as well as by the interaction with optical phonons and cannot be described on the basis of the uncoupled anisotropic model of Refs. 22 and 26. We predict that the $2S$ sublevel is the lowest excited state of the A exciton (see Table V). The splitting between the $2S$ and the optically allowed $2P_{\pm 1}$ substate, 0.86 meV, is smaller than the observed splitting between the $2P_{\pm 1}$ emission and the unknown emission line 1.3 meV below it (see Fig. 3). However, the calculated position of the $2S$ energy sublevel relative to the $n = 1$ state, 18.84 ± 0.2 meV, is in good agreement with the data of Ref. 24.

The value of the average "bare" hole mass $m_h = 0.476 m_0$ we have obtained from the value of the A-exciton effective Rydberg number $R_A = 21.1$ meV is smaller than those obtained in Ref. 9 from $R_A = 27.1$ meV. We have described the anisotropy of the hole effective masses in the A valence subband using only two unknown γ Luttinger parameters of the quasi–cubic approximation.[68] These parameters are determined by fitting experimental data. The resulting values of the parallel and perpendicular effective masses in the A valence subband are comparable with those obtained in Ref. 10. For the B and C valence subbands, the values of the hole effective masses depend crucially on the value of the crystal field energy and are given in the Table IV for a particular strain situation.

In conclusion, we have determined the fine structure of the A exciton and extracted values of the electron and hole effective g factors in wurtzite GaN (see Table III) using polarization-dependent and magnetoluminescence measurements. We have described the exciton energy level structure in wurtzite GaN as resulting from the combined effects of anisotropy, intersubband coupling, and polar interactions with optical phonons. From the analysis of our data, we were able to determine values of the exciton effective Rydberg numbers and to evaluate the effective mass and magnetic parameters for the valence band in wurtzite GaN (see Table IV).

APPENDIX A: EXPLICIT EXPRESSIONS

We give here explicit expressions for the functions appearing in the text.

1. $S_{n=1,2}$

The functions $S_{n=1,2}$ used in calculating the energy levels of the $1S$ and $2S$ states were defined in Ref. 27 and are given here for completeness:

$$S_n(x) = \sum_{n'=3}^{\infty} \frac{|I_{n'n}|^2}{x + 1/n^2 - 1/n'^2} + \int_0^{\infty} \frac{|I_{kn}|^2}{x + 1/n^2 + k^2}, \quad n = 1, 2, \quad \text{(A1)}$$

where

$$I_{n1} = \sqrt{\frac{n}{(n^2-1)(n^2-4)}} \left[3 - \frac{19n^2+5}{n^2-1} \left(\frac{n-1}{n+1} \right)^n \right], \quad \text{(A2)}$$

$$I_{k1} = \sqrt{\frac{k}{(k^2+1)(4k^2+1)C_k}} \times \left[3 + \frac{5k^2-19}{k^2+1} \exp\frac{-2\arctan(k)}{k} \right], \quad \text{(A3)}$$

$$I_{n2} = \sqrt{\frac{n}{(n^2-1)(n^2-4)}} \left[3 - \frac{135n^4-136n^2-80}{(n^2-4)^2} \left(\frac{n-2}{n+2} \right)^n \right], \quad \text{(A4)}$$

$$I_{k2} = \sqrt{\frac{k}{(k^2+1)(4k^2+1)C_k}} \times \left[3 + \frac{80k^4-136k^2-135}{(4k^2+1)^2} \exp\frac{-2\arctan(2k)}{k} \right], \quad \text{(A5)}$$

and $C_k = [1 - \exp(-2\pi/k)]$.

2. P_2^1 and P_2^3

The functions P_2^1 and P_2^3 used in calculating the energy levels of the $2P$ states are

$$P_2^1(x) = \sum_{n=3}^{\infty} \frac{|P_n^1|^2}{x + 1/4 - 1/n^2} + \int_0^{\infty} \frac{|P_k^1|^2}{x + 1/4 + k^2}, \quad \text{(A6)}$$

$$P_2^3(x) = \sum_{n=4}^{\infty} \frac{|P_n^3|^2}{x + 1/4 - 1/n^2} + \int_0^{\infty} \frac{|P_k^3|^2}{x + 1/4 + k^2}, \quad \text{(A7)}$$

where

$$P_n^1 = -\sqrt{\frac{2n(n^2-1)}{3}}\frac{128n}{5(n^2-4)^2}\left(\frac{n-2}{n+2}\right)^n, \quad n \geq 3,$$

$$P_2^1 = -\sqrt{15}, \tag{A8}$$

$$P_k^1 = -\sqrt{\frac{2k(k^2+1)}{C_k}}\frac{128}{5(4k^2+1)^2}\exp\frac{-2\arctan(2k)}{k}, \tag{A9}$$

$$P_n^3 = \sqrt{\frac{n}{14(n^2-1)(n^2-4)(n^2-9)}}\frac{n}{10}$$
$$\times\left[75 - \frac{3471n^4-5160n^2-336}{(n^2-4)^2}\left(\frac{n-2}{n+2}\right)^n\right], \tag{A10}$$

$$P_k^3 = \sqrt{\frac{k}{14(k^2+1)(4k^2+1)(9k^2+1)C_k}}$$
$$\times\left[\frac{15}{2} + \frac{336k^4-5160k^2-3471}{10(4k^2+1)^2}\exp\frac{-2\arctan(2k)}{k}\right]. \tag{A11}$$

3. $M_{n=1,2}$

The functions $M_{n=1,2}$ used in calculating the effective hole g factors of the $1S$ and $2S$ exciton states are

$$M_n(x) = \frac{1}{n}\sum_{n'=3}^{\infty}\frac{I_{n'n}L_{n'n}}{x+1/n^2-1/n'^2} + \frac{1}{n}\int_0^{\infty}\frac{I_{kn}L_{kn}}{x+1/n^2+k^2},$$
$$n=1,2, \tag{A12}$$

where

$$L_{n1} = \sqrt{n(n^2-1)(n^2-4)}\frac{8n^2}{(n^2-1)^3}\left(\frac{n-1}{n+1}\right)^n, \tag{A13}$$

$$L_{k1} = \sqrt{\frac{k(k^2+1)(4k^2+1)}{C_k}}\frac{8}{(k^2+1)^3}\exp\frac{-2\arctan(k)}{k}, \tag{A14}$$

$$L_{n2} = -\sqrt{n(n^2-1)(n^2-4)}\frac{2048n^2}{(n^2-4)^4}\left(\frac{n-2}{n+2}\right)^n, \tag{A15}$$

$$L_{k2} = \sqrt{\frac{k(k^2+1)(4k^2+1)}{C_k}}\frac{2048k^2}{(4k^2+1)^4}\exp\frac{-2\arctan(2k)}{k}. \tag{A16}$$

APPENDIX B: g-FACTOR OPERATOR

The orbital and anisotropic g–factor operators are

$$\hat{G}_{or}^{\parallel,\perp} = \begin{vmatrix} g_{or,A}^{\parallel,\perp}L_{z,x}\hat{T}_2 & 0 & 0 \\ 0 & g_{or,B}^{\parallel,\perp}L_{z,x}\hat{T}_2 & 0 \\ 0 & 0 & g_{or,C}^{\parallel,\perp}L_{z,x}\hat{T}_2 \end{vmatrix},$$

$$\hat{G}_{an} = \begin{vmatrix} g_A^{an}\tilde{L}_x\hat{T}_2 & 0 & 0 \\ 0 & g_B^{an}\tilde{L}_x\hat{T}_2 & 0 \\ 0 & 0 & g_C^{an}\tilde{L}_x\hat{T}_2 \end{vmatrix}, \tag{B1}$$

where $\mathbf{L}=[\mathbf{r}\times\mathbf{k}]$ is the orbital angular momentum operator, $\tilde{L}_x=(k_z y+k_y z)$, and

$$g_{or,v}^{\parallel} = \frac{m_0}{\tau_v^{\perp}}, \quad g_{or,v}^{\perp} = \frac{m_0}{2\sqrt{\eta}}\left[\frac{1}{\tau_v^{\perp}} + \frac{\eta}{\tau_v^{\parallel}}\right],$$

$$g_v^{an} = -\frac{m_0}{2\sqrt{\eta}}\left[\frac{1}{\tau_v^{\perp}} - \frac{\eta}{\tau_v^{\parallel}}\right],$$

$$\frac{1}{\tau_v^{\perp}} = \frac{1}{m_e^{\perp}} - \frac{1}{m_v^{\perp}}, \quad \frac{1}{\tau_v^{\parallel}} = \frac{1}{m_e^{\parallel}} - \frac{1}{m_v^{\parallel}}, \quad v=A,B,C. \tag{B2}$$

The coupling g–factor operators are

$$\hat{G}_{coup}^{\parallel\perp} = 3\gamma\times\begin{vmatrix} 0 & 0 & bQ_{1l}^{\parallel\perp} & aQ_{2l}^{\parallel\perp} & -aQ_{1l}^{\parallel\perp} & bQ_{2l}^{\parallel\perp} \\ 0 & 0 & aQ_{2l}^{\parallel\perp +} & -bQ_{1l}^{\parallel\perp +} & bQ_{2l}^{\parallel\perp +} & aQ_{1l}^{\parallel\perp +} \\ bQ_{1l}^{\parallel\perp +} & aQ_{2l}^{\parallel\perp} & 0 & 0 & abQ_l^{\parallel\perp} & -Q_{1l}^{\parallel\perp} \\ aQ_{2l}^{\parallel\perp +} & -bQ_{1l}^{\parallel\perp} & 0 & 0 & Q_{1l}^{\parallel\perp +} & abQ_l \\ -aQ_{1l}^{\parallel\perp +} & bQ_{2l}^{\parallel\perp} & abQ_l^{\parallel\perp} & Q_{1l}^{\parallel\perp} & 0 & 0 \\ bQ_{2l}^{\parallel\perp +} & aQ_{1l}^{\parallel\perp} & -Q_{1l}^{\parallel\perp +} & abQ_l^{\parallel\perp} & 0 & 0 \end{vmatrix}, \tag{B3}$$

where

$$Q_l^{\parallel}=L_z, \quad Q_l^{\perp}=\frac{1-2\eta}{2\sqrt{\eta}}L_x - \frac{1+2\eta}{2\sqrt{\eta}}\tilde{L}_x, \quad Q_{1l}^{\parallel}=-\frac{\sqrt{\eta}}{\sqrt{2}}r_-k_z, \quad Q_{1l}^{\perp}=\frac{1}{\sqrt{2}}(zk_z+yk_-),$$

$$Q_{2l}^{\parallel}=-ir_-k_-, \quad Q_{2l}^{\perp}=i\frac{z}{\sqrt{\eta}}k_-, \quad r_{\pm}=(x\pm iy). \tag{B4}$$

*On leave from A. F. Ioffe Physico-Technical Institute, 194021, St.-Petersburg, Russia.

[1] For a review, see S. Nakamura and G. Fasol, *The Blue Laser Diode* (Springer-Verlag, Berlin, 1997).

[2] M. Suzuki and T. Uenoyama, Jpn. J. Appl. Phys., Part 1 **34**, 3442 (1995); M. Suzuki, T. Uenoyama, and A. Yanase, Phys. Rev. B **52**, 8132 (1995).

[3] G.D. Chen, M. Smith, J.Y. Lin, H.X. Jiang, S. Wei, M. Asif Khan, and C.J. Sun, Appl. Phys. Lett. **68**, 2784 (1996).

[4] J.J. Pankove, S. Bloom, and G. Harbecke, RCA Rev. **36**, 163 (1975).

[5] U. Kaufmann, M. Kunzer, C. Merz, I. Akasaki, and H. Amano, Semicond. Sci. Technol. **11**, 712 (1996).

[6] M. Drechsler, D.M. Hoffmann, B.K. Meyer, T. Detchprohm, H. Amano, and I. Akasaki, Jpn. J. Appl. Phys., Part 2 **34**, L4 (1995).

[7] R.D. Cunningham, R.W. Brander, N.D. Knee, and D.K. Wickenden, J. Lumin. **5**, 21 (1972).

[8] J.S. Im, A. Moritz, F. Steuber, V. Härle, F. Scholz, and A. Hangleiter, Appl. Phys. Lett. **70**, 631 (1997).

[9] M. Steube, K. Reimann, D. Fröhlich, and S.J. Clark, Appl. Phys. Lett. **71**, 948 (1997).

[10] K. Kim, W.R.L. Lambrecht, B. Segall, and M. Schilfgaarde, Phys. Rev. B **56**, 7363 (1997).

[11] A. Hoffmann and L. Eckey, Mater. Sci. Forum **264-268**, 1259 (1998).

[12] R. Stepniewski, M. Potemski, A. Wysmalek, K. Pakula, J.M. Baranowski, J. Lusakowski, I. Grzegory, S. Porowski, G. Martinez, and P. Wyder, Phys. Rev. B **60**, 4438 (1999).

[13] A. Wysmalek, M. Potemski, R. Stepniewski, J. Lusakowski, K. Pakula, J.M. Baranowski, G. Martinez, P. Wyder, I. Grzegory, and S. Porowski, Phys. Status Solidi B **216**, 11 (1999).

[14] J. Campo, M. Julier, D. Coquillat, J.P. Lascaray, D. Scalbert, and O. Briot, Phys. Rev. B **56**, R7108 (1997).

[15] J. Flohrer, E. Jahnke, and M. Porsch, Phys. Status Solidi B **91**, 467 (1979).

[16] A.V. Rodina, M. Dietrich, A. Göldner, L. Eckey, Al.L. Efros, M. Rosen, A. Hoffmann, and B.K. Meyer, Phys. Status Solidi B **216**, 21 (1999).

[17] R. Stepniewski, K.P. Korona, A. Wysmalek, J.M. Baranowski, K. Pakula, M. Potemski, G. Martinez, I. Grzegory, and S. Porowski, Phys. Rev. B **56**, 15 151 (1997).

[18] B. Gil, O. Briot, and R.-L. Aulombard, Phys. Rev. B **52**, R17 028 (1995).

[19] W. Rieger, T. Metzger, H. Angerer, R. Dimitrov, O. Ambacher, and M. Stutzmann, Appl. Phys. Lett. **68**, 970 (1996).

[20] D. Volm, K. Oettinger, T. Streibl, D. Kovalev, M. Ben-Chorin, J. Diener, B.K. Meyer, J. Majewski, L. Eckey, A. Hoffmann, H. Amano, I. Akasaki, K. Hiramatsu, and T. Detchprohm, Phys. Rev. B **53**, 16 543 (1996).

[21] M. Julier, J. Campo, B. Gil, J.P. Lascaray, and S. Nakamura, Phys. Rev. B **57**, R6791 (1998).

[22] J.J. Hopfield and D.G. Thomas, Phys. Rev. **122**, 35 (1961).

[23] H. Venghaus, S. Suga, and K. Cho, Phys. Rev. B **16**, 4419 (1977).

[24] K. Kornitzer, T. Ebner, K. Thonke, R. Sauer, C. Kirchner, V. Schwegler, M. Kamp, and S. Porowski, Phys. Rev. B **60**, 1471 (1999).

[25] K. Kornitzer, T. Ebner, M. Grehl, K. Thonke, R. Sauer, C. Kirchner, V. Schwegler, M. Kamp, M. Leszczynski, I. Grzegory, and S. Porowski, Phys. Status Solidi B **216**, 5 (1999).

[26] R.G. Wheeler and J.O. Dimmock, Phys. Rev. **125**, 1805 (1962).

[27] A. Baldereschi and N.C. Lipari, Phys. Rev. B **3**, 439 (1971).

[28] M. Altarelli and N.C. Lipari, Phys. Rev. B **7**, 3798 (1973).

[29] L. Swierkowski, Phys. Rev. B **10**, 3311 (1974).

[30] K. Cho, S. Suga, W. Dreybrodt, and F. Willmann, Phys. Rev. B **11**, 1512 (1975).

[31] N.O. Lipari, Phys. Rev. B **4**, 4535 (1971).

[32] A.S. Barker, Jr. and M. Ilegems, Phys. Rev. B **7**, 743 (1973).

[33] T. Azuhata, T. Sota, K. Suzuki, and S. Nakamura, J. Phys.: Condens. Matter **7**, L129 (1995).

[34] H. Haken, Z. Phys. **146**, 527 (1957); Fortschr. Phys. **6**, 271 (1958).

[35] J. Pollmann and H. Büttner, Phys. Rev. B **16**, 4480 (1977).

[36] H. Fock, B. Kramer, and H. Büttner, Phys. Status Solidi B **67**, 199 (1975); *ibid.* **72**, 155 (1975).

[37] G. Behnke, H. Büttner, and J. Pollmann, Solid State Commun. **20**, 873 (1976).

[38] B. Pertzsch and U. Rössler, Phys. Status Solidi B **101**, 197 (1980).

[39] H.-R. Trebin, Phys. Status Solidi B **92**, 601 (1979).

[40] G.L. Bir and G.E. Pikus, *Symmetry and Strain-Induced Effects in Semiconductors* (Wiley, New York, 1974).

[41] J.M. Luttinger, Phys. Rev. **102**, 1030 (1956).

[42] L.D. Landau and E.M. Lifshitz, *Quantum Mechanics* (Pergamon Press, New York, 1989).

[43] A.M. Witowski, K. Pakula, J.M. Baranowski, M.L. Sadowski, and P. Wyder, Appl. Phys. Lett. **75**, 4154 (1999).

[44] Yong Zhang, A. Mascarenhas, and E.D. Jones, J. Appl. Phys. **83**, 448 (1998).

[45] R.A. Faulkner, Phys. Rev. **184**, 713 (1969).

[46] A. Baldereschi and M.G. Diaz, Nuovo Cimento Soc. Ital. Fis., B **68**, 217 (1970).

[47] P. Bigenwald and B. Gil (private communication).

[48] We note that the expressions for the intersubband coupling corrections to the *B*- and *C*-exciton states, obtained in second-order perturbation theory, can be used only if the separation between the interacting levels is not too small. For example, the function $S_1(x)$ must not be used for $[-1 < x < -0.82]$. This corresponds to a resonance interaction between the *C*-exciton ground state and the $n \geq 3$ discrete levels of the *A* or *B* excitons. The contribution of these resonance levels must be excluded from the function $S_1(x)$ and calculated by a direct diagonalization of the coupling matrix in first-order perturbation theory.

[49] K. Cho, Phys. Rev. B **10**, 4463 (1976).

[50] C. Weisbuch and R.G. Ulbrich, J. Lumin. **18/19**, 27 (1979).

[51] V.V. Travnikov and V.V. Krivolapchuk, Sov. Phys. JETP **58**, 1210 (1983).

[52] H. Sumi, J. Phys. Soc. Jpn. **41**, 526 (1976).

[53] B. Gil, A. Clur, and O. Briot, Solid State Commun. **104**, 267 (1997).

[54] I. Broser and M. Rosenzweig, Phys. Rev. B **22**, 2000 (1980).

[55] G. Blattner, G. Kurtze, G. Schmieder, and C. Klingshirn, Phys. Rev. B **25**, 7413 (1982).

[56] J. Röseler and K. Henneberger, Phys. Status Solidi B **93**, 213 (1979).

[57] K. Naniwae, S. Itoh, H. Amano, K. Itoh, K. Hiramatsu, and I. Akasaki, J. Cryst. Growth **99**, 381 (1990).

[58] A. Usui, H. Sunakawa, A. Sakai, and A.A. Yamaguchi, Jpn. J. Appl. Phys., Part 2 **36**, L899 (1997).

[59] H. Siegle, A. Hoffmann, L. Eckey, C. Thomsen, J. Christen, F. Bertram, D. Schmidt, D. Rudloff, and K. Hiramatsu, Appl. Phys. Lett. **71**, 2490 (1997).

[60] E. Gross, S. Permogorov, and B. Razbirin, J. Phys. Chem. Solids **27**, 1647 (1966).

[61] A. Hoffmann, Adv. Solid State Phys. **36**, 33 (1996).

[62] B.J. Skromme, Mater. Sci. Eng., B **50**, 117 (1997); B.J. Skromme, J. Jayapalan, R.P. Vaudo, and V.M. Phanse, Appl. Phys. Lett. **74**, 2358 (1999).

[63] G. Dresselhaus, A.F. Kip, and C. Kittel, Phys. Rev. **98**, 368 (1955).

[64] We note that the value of the hole parallel effective g factor $g_{A,1S}^{\parallel} = 1.1$ reported previously by our (Ref. 16) was obtained without comparison of the right- and left- circularly polarized spectra. In this work, additional experimental data were analyzed. The hole effective mass parameters were obtained in Ref. 16 using the Haken polaron model.

[65] W.E. Carlos, J.A. Freitas, Jr., M. Asif Khan, D.T. Olson, and J.N. Kuznia, Phys. Rev. B **48**, 17 878 (1993).

[66] D. Volm, T. Streibl, B.K. Meyer, T. Detchprohm, H. Amano, and I. Asasaki, Solid State Commun. **96**, 53 (1995).

[67] D.C. Reynolds, D.C. Look, W. Kim, U. Aktas, A. Botchkarev, A. Salvador, H. Morkoc, and D.N. Talwar, J. Appl. Phys. **80**, 594 (1996).

[68] We note that the difference between full wurtzite and quasicubic kinetic energy terms can be considered later within our approach as an additional perturbation.